CHEMISTRY
A EUROPEAN JOURNAL

DOI: 10.1002/chem.200900565

ESIMS Studies and Calculations on Alkali-Metal Adduct Ions of Ruthenium Olefin Metathesis Catalysts and Their Catalytic Activity in Metathesis Reactions

Hao-Yang Wang,[a, c] Wai-Leung Yim,[b, d] Thorsten Klüner,[b] and Jürgen O. Metzger*[a]

Abstract: Electrospray ionization mass spectrometry (ESIMS) and subsequent tandem mass spectrometry (MS/MS) analyses were used to study some important metathesis reactions with the first-generation ruthenium catalyst **1**, focusing on the ruthenium complex intermediates in the catalytic cycle. In situ cationization with alkali cations (Li^+, Na^+, K^+, and Cs^+) using a microreactor coupled directly to the ESI ion source allowed mass spectrometric detection and characterization of the ruthenium species present in solution and particularly the catalytically active monophosphine–ruthenium intermediates present in equilibrium with the respective bisphosphine–ruthenium species in solution. Moreover, the intrinsic catalytic activity of the cationized monophosphine–ruthenium complex **1a**·K^+ was directly demonstrated by gas-phase reactions with 1-butene or ethene to give the propylidene Ru species **3a**·K^+ and the methylidene Ru species **4a**·K^+, respectively. Ring-closing metathesis (RCM) reactions of 1,6-heptadiene (**5**), 1,7-octadiene (**6**) and 1,8-nonadiene (**7**) were studied in the presence of KCl and the ruthenium alkylidene intermediates **8**, **9**, and **10**, respectively, were detected as cationized monophosphine and bisphosphine ruthenium complexes. Acyclic diene metathesis (ADMET) polymerization of 1,9-decadiene (**14**) and ring-opening metathesis polymerization (ROMP) of cyclooctene (**18**) were studied analogously, and the expected ruthenium alkylidene intermediates were directly intercepted from reaction solution and characterized unambiguously by their isotopic patterns and ESIMS/MS. ADMET polymerization was not observed for 1,5-hexadiene (**22**), but the formation of the intramolecularly stabilized monophosphine ruthenium complex **23a** was seen. The ratio of the signal intensities of the respective with potassium cationized monophosphine and bisphosphine alkylidene Ru species varied from $[I_{4a}]/[I_4] = 0.02$ to $[I_{23a}]/[I_{23}] = 10.2$ and proved to be a sensitive and quantitative probe for intramolecular π-complex formation of the monophosphine–ruthenium species and of double bonds in the alkylidene chain. MS/MS spectra revealed the intrinsic metathesis catalytic activity of the potassium adduct ions of the ruthenium alkylidene intermediates **8a**, **9a**, **10a**, **15a**, and **19a**, but not **23a** by elimination of the respective cycloalkene in the second step of RCM. Computations were performed to provide information about the structures of the alkali metal adduct ions of catalyst **1** and the influence of the alkali metal ions on the energy profile in the catalytic cycle of the metathesis reaction.

Keywords: alkali metals · cations · mass spectrometry · olefination · pi interactions · reactive intermediates

Introduction

Ruthenium–carbene-based olefin metathesis is a powerful reaction for the formation of carbon–carbon double bonds in organic and polymer synthesis.[1,2] The reaction mechanism was studied most thoroughly, because detailed knowledge is of great importance in general and with respect to industrial applications. Many details are known on the vari-

[a] Dr. H.-Y. Wang, Prof. Dr. J. O. Metzger
Institute of Pure and Applied Chemistry
University of Oldenburg
Carl-von-Ossietzky-Str. 9-11, 26129 Oldenburg (Germany)
Fax: (+49) 441-798-193718
E-mail: Juergen.Metzger@uni-oldenburg.de

[b] Dr. W.-L. Yim, Prof. Dr. T. Klüner
Department of Theoretical Chemistry, University of Oldenburg
Carl-von-Ossietzky-Str. 9-11, 26129 Oldenburg (Germany)

[c] Dr. H.-Y. Wang
Shanghai Mass Spectrometry Center
Shanghai Institute of Organic Chemistry
Lingling Road 345, Shanghai 200032 (China)

[d] Dr. W.-L. Yim
Institute of High Performance Computing
1 Fusionopolis Way, #16-16 Connexis, Singapore 138632 (Singapore)

Supporting information for this article is available on the WWW under http://dx.doi.org/10.1002/chem.200900565.

ous versions of metathesis such as homo- and cross-metathesis, ring-closing metathesis (RCM), ring-opening metathesis polymerization (ROMP), and acyclic diene metathesis (ADMET) polymerization.

The development of mass spectrometric ionization methods at atmospheric pressure (API) like electrospray ionization (ESI) enable the investigation of liquid solutions by mass spectrometry and open up access to the direct investigation of chemical reactions in solution using mass spectrometry (MS).[3] In principle, they make the detection and study not only of reaction substrates and products but even of short-lived reaction intermediates as they are present in solution possible[4] and provide new insights into the mechanism of the reactions studied, including important homogeneously catalyzed reactions.[5]

Chen used ESIMS for the study of metathesis reaction primarily in the gas phase.[6,7] Electrospray transfers charged species from solution to the gas phase; therefore, the neutral ruthenium metathesis catalysts such as **1** (Scheme 1) have to be derived with a charge to become a selective probe. Chen developed two protocols to do that. Firstly, he used a first-generation catalyst with charged phosphine ligands developed by Grubbs et al. for water-soluble ruthenium catalysts[8] and investigated some important aspects of metathesis reactions in the gas phase. Thus, he could generate 14-electron Ru species by collision-induced dissociation (CID) of 16-electron Ru species and demonstrate their catalytic activity in cross metathesis reactions with ethene and 1-butene, as well as in ROMP with cyclobutene, cyclopentene, and norbornene.[7] Secondly, he trapped the catalytically active species in the ROMP of norbornene in solution with a cationized substrate. The mass spectra obtained corresponded to the selective detection of the catalyst-bound, charge-labeled substrate. Moreover, it was claimed that the observed species should represent the resting state of the complex involved in the catalytic cycle.[6,9]

It is of high interest to be able to investigate by MS the on-going metathesis reaction in solution. Recently, we reported that reactions of first-generation ruthenium olefin metathesis catalysts **1** and **2** (Scheme 1) in solution can be successfully studied on-line by ESIMS.[10] It was possible to detect and characterize 14-electron monophosphine–ruthenium intermediates directly from solution. Moreover, the catalytic activity of these species was demonstrated by gas-phase reactions with ethene. We used the in situ exchange of a neutral phosphine ligand against a "charge-labeled" phosphine to be able to detect the neutral Ru species. We studied some examples of ring-closing metathesis reactions in solution. Unfortunately, the alkylidene intermediates in the catalytic cycle with the exception of the methylidene Ru species **4** ($[Cl_2(PCy_3)_2Ru{=}CH_2]$, Cy = cyclohexane) could not be detected.

The use of the "charge-labeled" phosphine has some disadvantages. The excess of phosphine present in solution will change the reaction conditions in comparison to the synthesis protocol normally used.[11] Moreover, this technique cannot be used to study the catalytically active Ru species of second-generation catalysts and Hoveyda–Grubbs catalysts.

We thought it would be of wide interest to develop a much simpler and more generally applicable method to study the metathesis reaction in solution by the powerful tool of mass spectrometry. Therefore, we would need a simple process to convert the neutral ruthenium catalyst **1** into an ionic species suited for mass spectrometric investigations with retention of the catalytic activity. It has been shown that metallation, the formation of metal-ion adducts, is a favorable process for converting neutral inorganic or organometallic molecules into cationic derivatives.[13] For example, after simple addition of sodium salts, the neutral anticancer drugs tetraplatin and cisplatin both gave peaks in the ESI mass spectra corresponding to sodium-ion adducts. Presumably, in these compounds, adduction occurs through the halogen atom.[14] We have observed that this simple cationization with alkali-metal cations is also possible with **1** and enables the detection and the study of this important catalyst.

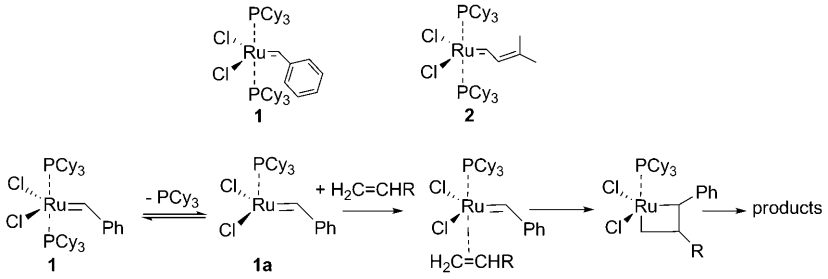

Scheme 1. First-generation Ru catalysts **1** and **2** and most favorable catalytic metathesis pathway of **1** and an alkene through phosphine dissociation of **1**, *trans*-addition of the alkene, formation of the metallocyclobutane intermediate, cycloreversion, and formation of the products.[17c,d]

Alkali-metal cationization has been used for mass spectrometric characterization of not only organic compounds,[12] but also organometallic compounds.[13–15] The addition of Na^+ has been used to characterize a range of neutral rhenium–bipyridine complexes[14] and Henderson et al. observed alkali-metal (Li^+, Na^+, and K^+) adduct ions with Ru carbonyl compounds and suggested that such electron-rich compounds have sufficient charge residing on the CO ligands to enable attachment to the cation.[15] Grubbs et al. used alkali-metal ions as templates to direct the RCM reaction to the formation of unsaturated crown ether analogues,[16] which demonstrates that the introduction of alkali-metal ions would not block the metathesis activity of cata-

lyst. However, alkali-metal cationization has not been applied to the mass spectrometric investigation of Ru-catalyzed metathesis reactions.

Herein, we studied the first-generation catalyst **1** in solution by ESIMS and ESI tandem mass spectrometry (ESIMS/MS) with the aim to elucidate the scope of this method and to investigate some important examples of metathesis reaction such as RCM, ROMP, and ADMET polymerization, and to detect and to characterize the intermediates in the catalytic cycle from the reaction solution. Moreover, computations on ruthenium–carbene complexes will help to understand the complex reaction sequence. It has been shown that the dissociative pathway of first-generation Ru catalysts with *trans*-addition of the alkene is most favored (Scheme 1).[17] Thus, we studied by quantum-mechanical calculations the effect of the alkali cation on the energetics of the catalytically active Ru species.

Results

ESIMS study of the ruthenium catalyst 1 in the presence of alkali-metal ions: We mixed one equivalent of the Ru catalyst **1** dissolved in CH_2Cl_2 with five equivalents of LiCl dissolved in methanol using a microreactor directly coupled to the ESI source. Methanol was used because of the solubility of alkali chlorides in this solvent. The injection speed of both solutions was set at 5 μL min^{-1}, allowing the study of the solution after a reaction time of approximately 12 s. The ESI spectrum obtained revealed the formation of **1**·Li$^+$ at *m*/*z* 829 which could be identified through the characteristic isotopic pattern.[18] The signal of radical cation **1**$^{\cdot+}$ at *m*/*z* 822 was detected with low intensity, the ratio of the intensities of *m*/*z* 822 and *m*/*z* 829 was about 0.002. The $[(PCy_3)_2ClRu{=}CHPh]^+$ ion (Ph = phenyl; [**1**−Cl]$^+$), formed by dissociation of chloride in solution, was observed at *m*/*z* 787. The ratio of the intensities of the signals of **1**·Li$^+$ and [**1**−Cl]$^+$ was 0.45. The increased relative intensity of the [**1**−Cl]$^+$ ion at *m*/*z* 787 compared with the signal observed in CH_2Cl_2 may be due to the enhanced heterolysis induced by adding CH_3OH and LiCl.[10,18] In addition, the cationized dimer **1**$_2$·Li$^+$ at *m*/*z* 1651 was detected with low intensity ([**1**$_2$·Li$^+$]/[**1**] = 0.001). The base peak at *m*/*z* 281 is the signal of ion $Cy_3P{\cdot}H^+$.[10] Remarkably, the Li$^+$ adduct ion of the 14-electron Ru species **1a** (Scheme 1), formed by dissociation of Cy_3P, could be detected at *m*/*z* 549 with a low intensity of [**1a**·Li$^+$]/[**1**·Li$^+$] = 0.005 unambiguously, as well as [**1a**−Cl]$^+$ at *m*/*z* 507 ([**1a**−Cl]$^+$]/[**1a**·Li$^+$] = 0.3). A signal for lithium-cationized Cy_3P was not observed. The ion $Cy_3P^+CH_2Ph$ at *m*/*z* 371 was also detected with low intensity, and it has been reported by us to be a decomposition product of catalyst **1**.[10] The respective alkali-metal adduct ions of catalyst **1** were obtained in the presence of NaCl, KCl or CsCl.[18] In Scheme 2, the observed Ru carbene species are summarized having been unambiguously detected and characterized by their isotopic patterns and by CID.

The ESIMS/MS spectra for the CID of **1**·M$^+$ (M = Li, Na, K, Cs; Figure 1) showed two main fragments due to the loss of PCy_3 and of MCl, respectively, using a collision energy of 8 or 10 eV. Interestingly, going from Li$^+$ to Na$^+$ to K$^+$ and finally to Cs$^+$, the intensity ratio of the fragment ions [**1**·M−MCl]$^+$/[**1**·M−PCy$_3$]$^+$ decreased by more than two orders of magnitude going from 17.5 to 2.33 to 0.24 and finally to 0.11, respectively. Only a 2 eV collision energy could cause the dissociation of ions **1a**·M$^+$. Figure 2 a–d show the fragmentation ion series of **1a**·M$^+$ at *m*/*z*: a) 457, 455 and 419; b) 473, 471 and 435; c) 489, 487 and 451; and d) 583, 581 and 545 by loss of the benzylidene ligand as C_7H_8 (−92 u) and C_7H_8+H_2 (−94 u) and further by loss of HCl (−36 u) with low intensity. Going from Li$^+$ to Na$^+$ to K$^+$ and finally to Cs$^+$, the intensity ratio of the fragment ions [**1a**·M−(C_7H_8+H_2)]$^+$/[**1a**·M−C_7H_8]$^+$ decreased from

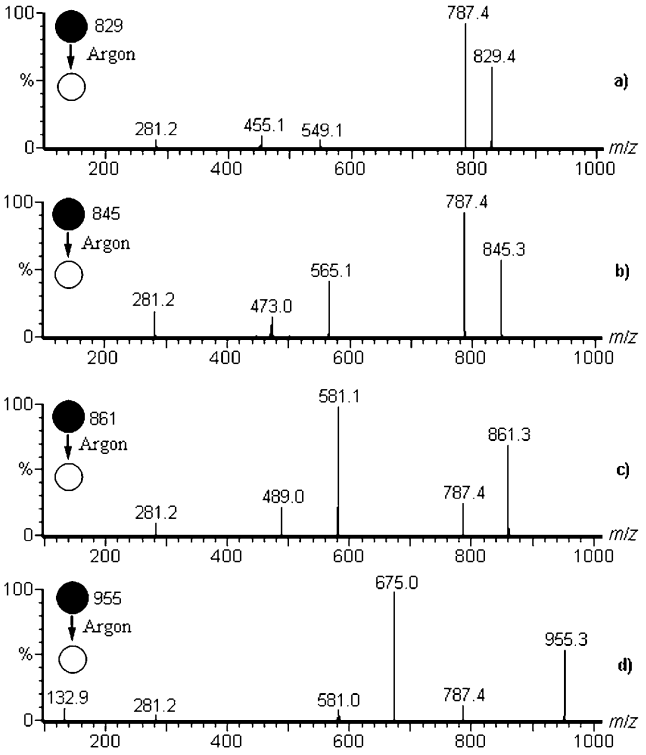

Figure 1. ESIMS/MS spectra for the CID of: a) **1**·Li$^+$ at *m*/*z* 829, collision energy of 8 eV; b) **1**·Na$^+$ at *m*/*z* 845, collision energy of 8 eV; c) **1**·K$^+$ at *m*/*z* 861, collision energy of 9 eV; d) **1**·Cs$^+$ at *m*/*z* 955, collision energy of 10 eV.

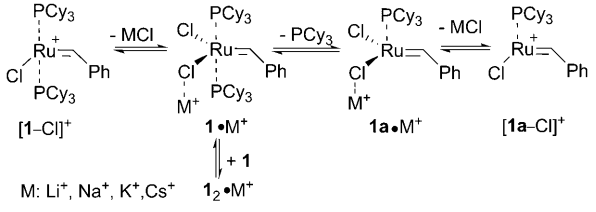

Scheme 2. Ru–carbene species derived from complex **1**·M$^+$ observed by ESIMS.

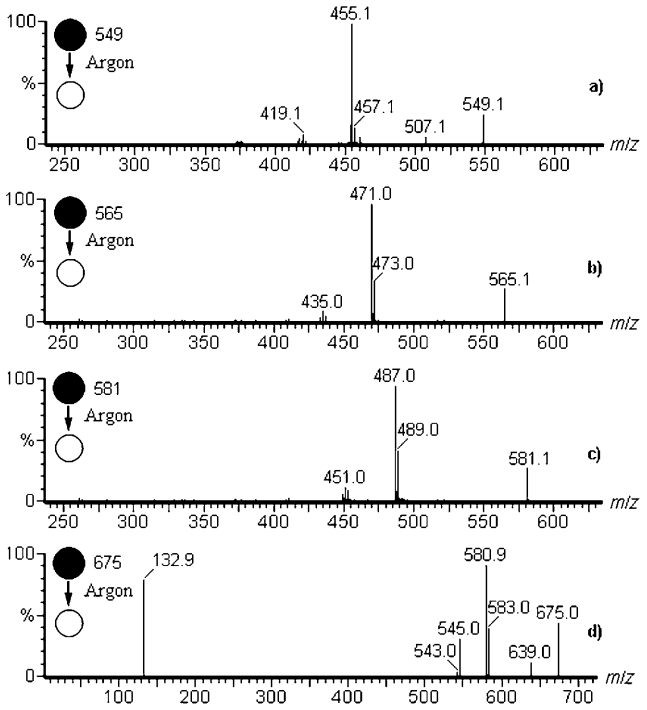

Figure 2. ESIMS/MS spectra for the CID of: a) **1a**·Li$^+$ at *m*/*z* 549; b) **1a**·Na$^+$ at *m*/*z* 565; c) **1a**·K$^+$ at *m*/*z* 581; d) **1a**·Cs$^+$ at *m*/*z* 675, collision energy of 2 eV.

8.5 to 2.9 to 2.4 and finally to 2.2, respectively. The Li$^+$ adduct shows additionally loss of LiCl. Some analogous results were obtained using catalyst **2**.[18]

Gas-phase ion–molecule reactions of the Li$^+$ or K$^+$ adduct ions of 1 and 1a with olefins: Being able to detect the alkali-metal adduct ions of Ru species **1** and **1a**, we wanted to directly probe their catalytic activities[19] by ion–molecule reactions in the gas phase[7,10]. This was performed in the collision-cell of the quadrupole time of flight (Q-TOF) mass spectrometer using the gas-phase reaction of a monoisotopic ion (selected in the quadrupole) with 1-butene or ethene with mass analysis of the product ions using the time of flight (TOF) analyzer. We selected the Li$^+$ and K$^+$ adduct ions as examples. As expected, the bisphosphine Ru species **1**·Li$^+$ at *m*/*z* 829 and **1**·K$^+$ at *m*/*z* 861 did not show metathesis reactions with 1-butene or ethene.[18]

In contrast, the mass-selected monophosphine Ru species **1a**·K$^+$ at *m*/*z* 581 reacted under low-energy collisions (0.5 eV) in the collision-cell (quenched by low-energy collisions with the neutral 1-butene) with 1-butene yielding the propylidene Ru complex ion **3a**·K$^+$ at *m*/*z* 533 (relative intensity 4.4%) and additionally the ions at *m*/*z* 487, 489, and 545 (Figure 3a). The tendency of the ion–molecule reaction of **1a**·K$^+$ with ethene is much lower in comparison to 1-butene, yielding methylidene Ru complex ion **4a**·K$^+$ at *m*/*z* 505 (relative intensity: 0.4%) and ions at 487, 489, and 517 (Figure 3b). Comparison with the ESIMS/MS spectrum of **1a**·K$^+$ (Figure 2c) revealed that the ions at *m*/*z* 487 and 489

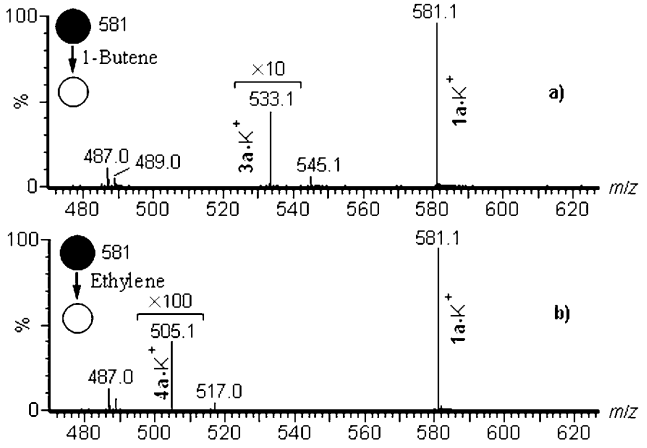

Figure 3. Mass spectra of ion–molecule reactions of **1a**·K$^+$ at *m*/*z* 581 with: a) 1-butene (the intensity of **3a**·K$^+$ at *m*/*z* 533 was enhanced ×10); b) ethene (the intensity of **4a**·K$^+$ at *m*/*z* 505 was enhanced ×100), collision energy of 0.5 eV.

are fragment ions, whereas *m*/*z* 545 or 517 were likely product ions of the reaction of the fragment ion at *m*/*z* 489 with 1-butene and ethene, respectively, as reported previously (Scheme 3).[10]

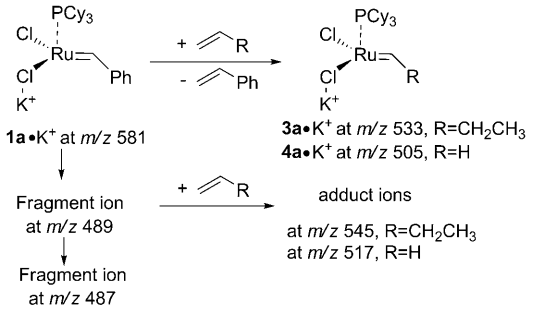

Scheme 3. Ion–molecule reactions of **1a**·K$^+$ with 1-butene or ethene.

The rate of the reaction of **1a**·Li$^+$ and 1-butene to give the metathesis product ion **3a**·Li$^+$ at *m*/*z* 501 (relative intensity: 0.2%) is about one order of magnitude lower than that of **1a**·K$^+$, and the metathesis product ion **4a**·Li$^+$ at *m*/*z* 473 was not observed in the reaction of **1a**·Li$^+$ with ethene. A π-complex of **1a**·M$^+$ and alkene, or a ruthenacyclobutane, neither with 1-butene nor ethene could be detected. Interestingly, the ion–molecule reaction of [**1a**−Cl]$^+$ at *m*/*z* 507 with ethene did not show any metathesis products but gave the adduct ion of ethene at *m*/*z* 535, which demonstrated that these ion species were able to coordinate an alkene to the free coordination site of Ru, but without metathesis catalytic activity.[18]

The results reported above gave evidence that the catalytic activities were retained in the alkali metal cationized monophosphine complexes **1a**·M$^+$. The K$^+$ adduct ions showed higher catalytic activity than the Li$^+$ analogues, thus KCl was used as the cationization agent to intercept the

neutral Ru intermediates in olefin metathesis reaction solutions of **1** with different olefins.

Ru–carbene intermediates in ring-closing olefin metathesis (RCM) reactions: The well-accepted mechanism of the RCM reaction is shown in Scheme 4.[20] We reacted one

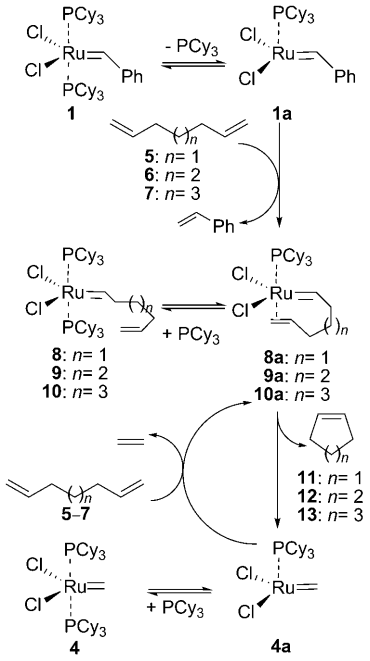

Scheme 4. The catalytic cycle of RCM reaction of α,ω-dienes **5–7** catalyzed by **1**.[20]

equivalent of catalyst **1** dissolved in CH_2Cl_2 with 20 equivalents of an acyclic diene, 1,6-heptadiene (**5**), 1,7-octadiene (**6**), or 1,8-nonadiene (**7**), and five equivalents of KCl dissolved in methanol, using a microreactor directly coupled to the ESI source. The injection speed of both solutions was set at 5 μL min^{-1}, which allowed the study of the reaction mixture at room temperature after a reaction time of 12 s. Remarkably, the K^+ adduct ions of bis- and monophosphine–alkylidene–Ru intermediates **8–10** and **8a–10a**, respectively, and methylidene–Ru intermediates **4** as well as **4a** were detected from the RCM reaction solutions directly (Scheme 4) and characterized by their MS/MS spectra; **10** and **10a** were further characterized by their isotopic patterns.[18] The ratios of the intensities of the mono- and bisphosphine–alkylidene–Ru intermediates are compiled in Table 1. Most interestingly, the ESIMS/MS spectrum of **8a**·K^+ at *m*/*z* 573 revealed that **8a**·K^+ underwent a gas phase RCM reaction to give the methylidene–Ru complex **4a**·K^+ at *m*/*z* 505 by eliminating cyclopentene (**11**) using very low collision energy (0.5 eV, Figure 4a). The respective reactions were observed as well after performing a MS/MS on **9a**·K^+ at *m*/*z* 587 and on **10a**·K^+ at *m*/*z* 601. Interestingly, the rate of the gas phase RCM of **8a**·K^+ and of **10a**·K^+, which eliminated cyclopentene (**11**) and cycloheptene (**13**),

Table 1. Ratios of the intensities of mono- and bisphosphine–Ru complexes in various metathesis reaction systems.

Reactions	Bisphosphine Ru complex (*m*/*z*)	Monophosphine Ru complex (*m*/*z*)	I_M/I_B[c]
1 @ LiCl[a]	**1**·Li^+ (829)	**1a**·Li^+ (549)	0.005
1 @ NaCl[a]	**1**·Na^+ (845)	**1a**·Na^+ (565)	0.02
1 @ KCl[a]	**1**·K^+ (861)	**1a**·K^+ (581))	0.03
1 @ CsCl[a]	**1**·Cs^+ (955)	**1a**·Cs^+ (675)	0.05
1 with **5** @ KCl[b]	**8**·K^+ (853)	**8a**·K^+ (573)	0.7
1 with **6** @ KCl[b]	**9**·K^+ (867)	**9a**·K^+ (587)	0.3
1 with **7** @ KCl[b]	**10**·K^+ (881)	**10a**·K^+ (601)	0.5
1 with **6** @ KCl[b]	**4**·K^+ (785)	**4a**·K^+ (505)	0.02
	15·K^+ (895)	**15a**·K^+ (615)	0.5
1 with **14** @ KCl[b]	**16**·K^+ (1005)	**17a**·K^+ (725)	0.2
	17·K^+ (1115)	**18a**·K^+ (835)	0.4
	19·K^+ (971)	**19a**·K^+ (691)	2.1
1 with **18** @ KCl[b]	**20**·K^+ (1081)	**20a**·K^+ (801)	0.4
	21·K^+ (1191)	**21a**·K^+ (911)	0.4
1 with **22** @ KCl[b]	**23**·K^+ (839)	**23a**·K^+ (559)	10.2

[a] A solution of **1** in CH_2Cl_2 was mixed with a CH_3OH solution of the alkali metal salt. [b] The reaction of **1** with the substrate was performed in the presence of a CH_3OH solution of the alkali metal salt. [c] Ratio of mono- and bisphosphine–Ru complex.

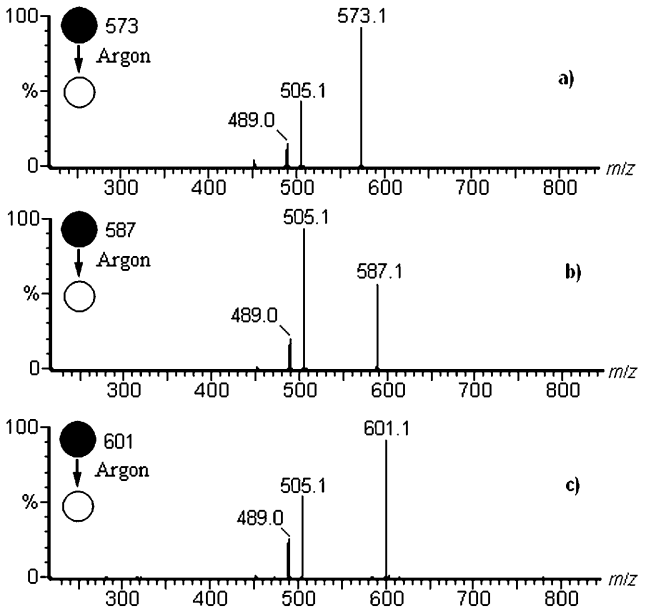

Figure 4. ESIMS/MS spectra for the CID of: a) **8a**·K^+ at *m*/*z* 573; b) **9a**·K^+ at *m*/*z* 587; c) **10a**·K^+ at *m*/*z* 601, collision energy of 0.5 eV.

respectively, was similar, but slower than that of **9a**·K^+, which eliminated cyclohexene (**12**, Figure 4).

ADMET polymerization of 1,9-decadiene (14): The mechanism of ADMET polymerization of 1,9-decadiene (**14**) with **1** is given in Scheme 5.[21] We studied this reaction by reacting one equivalent of the Ru catalyst **1** in CH_2Cl_2 with 20 equivalents of **14** and five equivalents of KCl in methanol, using a microreactor directly coupled to the ESI source, which allowed the study of the reaction mixture at room temperature after a reaction time of 12 s. The first intermediate (**15**) was detected as **15**·K^+ at *m*/*z* 895 as well as

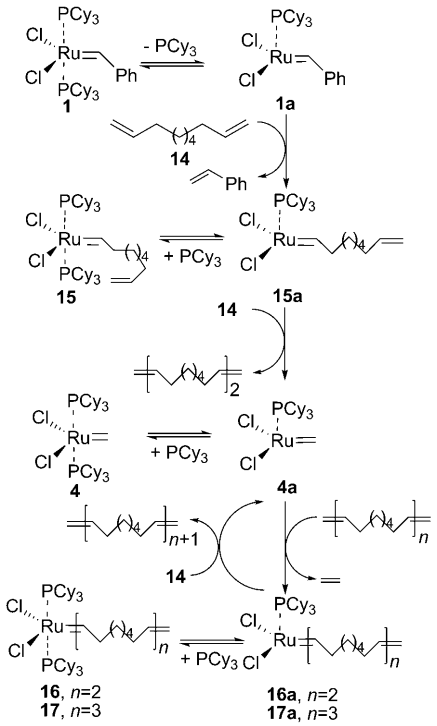

Scheme 5. The catalytic cycle of ADMET polymerization reaction of 1,9-decadiene (**14**) with **1**.[21]

15a·K$^+$ at *m*/*z* 615 in the very first seconds of the reaction, whereas the higher alkylidene–Ru intermediates **16a**·K$^+$, **16**·K$^+$, **17a**·K$^+$, and **17**·K$^+$ as well as the methylidene–Ru intermediates **4**·K$^+$ and **4a**·K$^+$ could be observed clearly after a reaction time of 1 h in the ESI mass spectrum, while the signal of the **1**·K$^+$ at *m*/*z* 861 disappeared (Scheme 5). The ratios of the intensities of the mono- and the respective bisphosphine–Ru species **15**·K$^+$–**17**·K$^+$ and **4**·K$^+$are given in Table 1. The **15a**·K$^+$ species at *m*/*z* 615 underwent a gas-phase RCM reaction in MS/MS, eliminating cyclooctene (**18**) at a very low collision energy of 0.5 eV to give the ion **4a**·K$^+$ at *m*/*z* 505 (Figure 5a).

The relative intensity of the product ion **4a**·K$^+$ was significantly lower compared to the gas-phase RCM reaction tendency of the ions **8a**·K$^+$–**10a**·K$^+$ (Figure 4), suggesting that the intrinsic tendency of the formation of the eight-membered ring is much lower than that of the formation of five-, six- and seven-membered rings. These results are in good agreement with previous reports in the solution phase, which showed that the formation of eight-membered rings through RCM only occurs in systems in which the dienes are conformationally predisposed to ring formation.[22] The ions **16a**·K$^+$ at *m*/*z* 725 and **17a**·K$^+$ at *m*/*z* 835 needed a higher collision energy of 2 eV and showed twofold and threefold elimination of cyclooctene (**18**) in MS/MS, respectively (Figure 5b,c).

ROMP reactions of cyclooctene (18): The mechanism of the ROMP[23] of cyclooctene (**18**) with **1** is given in Scheme 6. We studied this reaction by reacting one equivalent of the

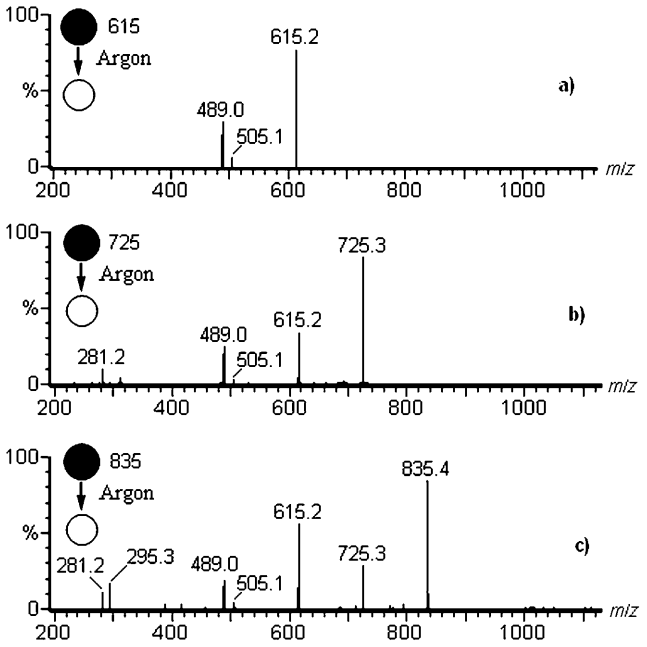

Figure 5. ESIMS/MS spectra for the CID of: a) **15a**·K$^+$ at *m*/*z* 615, collision energy of 0.5 eV; b) **16a**·K$^+$ at *m*/*z* 725, collision energy at 2 eV; c) **17a**·K$^+$at *m*/*z* 835, collision energy of 2 eV.

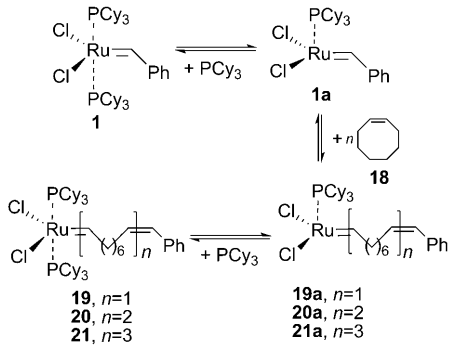

Scheme 6. ROMP reaction of cyclooctene (**18**) with the Ru catalyst **1**.[23]

Ru catalyst **1** in CH_2Cl_2 with 20 equivalents of cyclooctene and five equivalents of KCl in methanol, using a microreactor directly coupled to the ESI source. Our experimental results showed that the ROMP was initiated faster than the ADMET polymerization and the propagating alkylidene–Ru intermediates **19–21** and **19a–21a**, respectively (Scheme 6), were detected as their K$^+$ adduct ions just after a reaction time of 12 s. The ratios of the intensities of the respective mono- and bisphosphine–Ru species are given in Table 1.

Interestingly, the ESIMS/MS spectrum of **19a**·K$^+$ at *m*/*z* 691 showed a loss of cyclooctene (**18**) to give **1a**·K$^+$ at *m*/*z* 581 at a very low collision energy of 0.5 eV, which is evidently the gas-phase RCM back-reaction of the first step of solution-phase ROMP (Figure 6a). The MS/MS spectra of **20a**·K$^+$ at *m*/*z* 801 and **21a**·K$^+$ at *m*/*z* 911 exhibited the eliminations of two and three cyclooctene units, respectively, (Figure 6b,c) similar to the fragmentation of **16a**·K$^+$ and

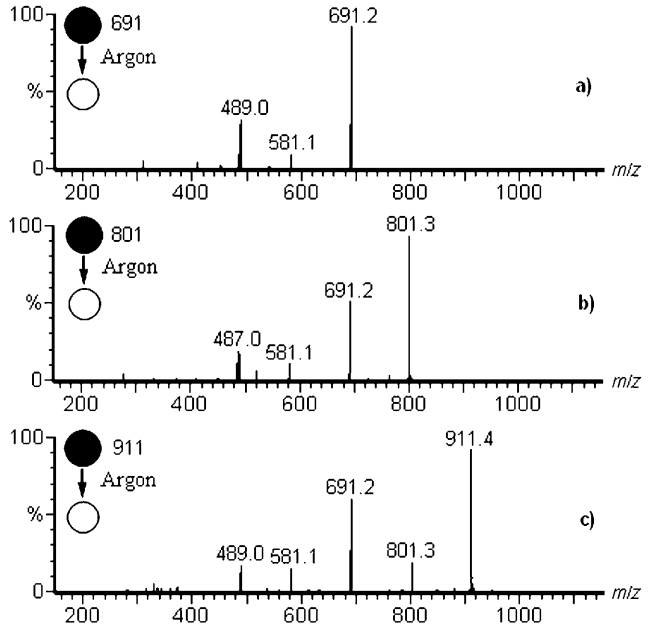

Figure 6. ESIMS/MS spectra for the CID of: a) **19a**·K^+at *m/z* 691, collision energy of 0.5 eV; b) **20a**·K^+at *m/z* 801, collision energy of 2 eV; c) **21a**·K^+at *m/z* 911, collision energy of 2 eV.

17a·K^+ (Figure 5b,c) at a higher, but still relatively low, collision energy of 2 eV.

Reaction of 1,5-hexadiene with catalyst 1: It is known that the RCM reaction giving a four-membered ring is not possible because of the highly strained ring.[2] It is known as well that ADMET polymerization of 1,5-hexadiene (**22**) is sluggish and preferentially cyclooctadiene is formed.[24] In order to check whether four-membered ring formation could occur in a gas phase through a RCM reaction, we studied the metathesis reaction of 1,5-hexadiene (**22**) with **1** in the presence of KCl (Scheme 7).

We did not detect chain-propagating alkylidene–Ru intermediates in ADMET, even with long reaction times (1 or 2 h). This is in agreement with previous reports that the Ru-catalyzed 1,5-hexadiene polymerization produces much lower molecular-weight polymer in lower yield and occurs more slowly than that of 1,9-decadiene. However, we found

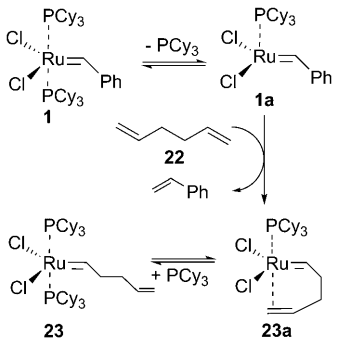

Scheme 7. Reaction of 1, 5-hexadiene (**22**) with the Ru catalyst **1**.[22]

some interesting "abnormal" phenomena: the ratio of the intensities of **23a**·K^+/**23**·K^+ = 10.2 was remarkably higher by two orders of magnitude than in a normal system without intramolecular π complexation, such as **1a**·K^+/**1**·K^+ = 0.03 (Table 1) and the energy of 16 eV necessary for CID of **23a**·K^+ was significantly higher than that for other K^+ adduct ions of monophosphine–Ru complexes (0.5–2 eV). These results provide clear evidence that intramolecular π -complexation within **23a** significantly increased the stability of the monophosphine –Ru complex and at the same time decreased the metathesis activity by preventing the Ru center to access and react with olefin molecules,[22] which has also been hypothesized by Grubbs et al. and is similar to the negative neighboring group effect observed for dienes containing heteroatoms.[25] The extremely high collision energy (16 eV) and the formation of protonated tricyclohexylphosphine *m/z* 281 show the great difference between complex **23a**·K^+ and other monophosphine complexes which have been studied. The absence of **4a**·K^+ at *m/z* 505 in the MS/MS spectrum of **23a**·K^+ at *m/z* 559 in Figure 7b demonstrated that the formation of a highly strained four-membered ring through a RCM reaction did not occur even under gas-phase conditions.

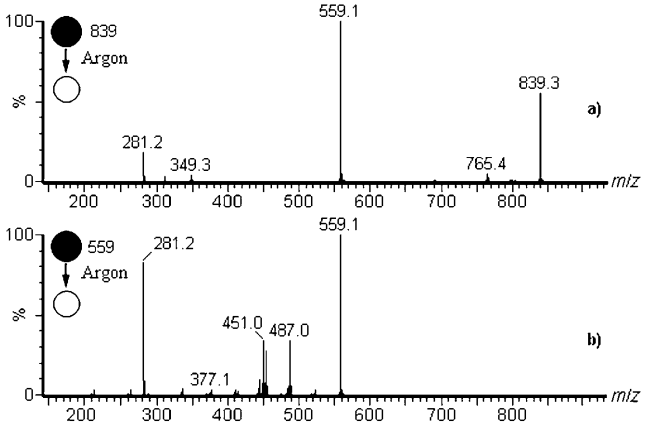

Figure 7. ESIMS/MS spectra for the CID of: a) **23**·K^+at *m/z* 839, collision energy of 8 eV; b) **23a**·K^+at *m/z* 559, collision energy of 16 eV.

Computational results: We performed theoretical calculations for the structures and relative energies of the Li^+ and K^+ adduct ions of the Ru catalyst **1** and studied the energetic profiles of the metathesis reactions of the monophosphine Ru species **1a**, **1a**·Li^+ or **1a**·K^+ with ethene. Figure 8 shows the calculated structures of **1**·Li^+ and **1**·K^+ and the energy landscape is illustrated in Figure 9, in which, in order to facilitate the comparison of the different reactions, the energy of state 2 was set as the reference point for all the three cases: Li^+ adduct ions, K^+ adduct ions, and bare complexes. The important energy changes during the metathesis reactions are summarized in Table 2 and further details of the computational results including energy and structure information of intermediates are given in the supporting information.[18]

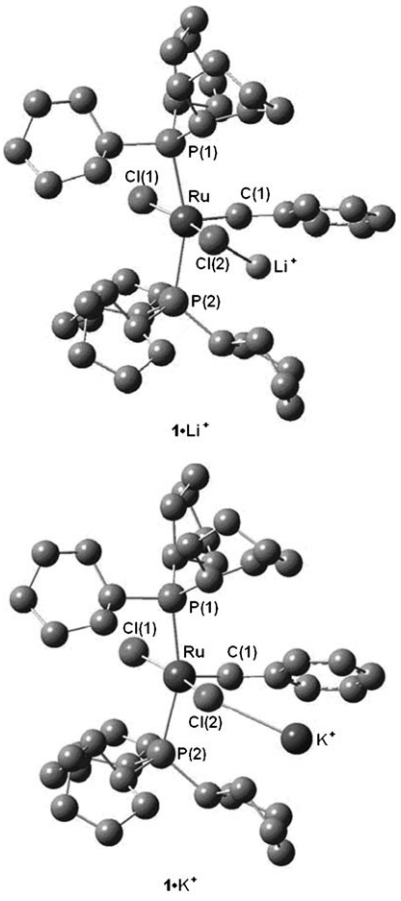

Figure 8. Ball and stick models of $\mathbf{1}\cdot Li^+$ and $\mathbf{1}\cdot K^+$.

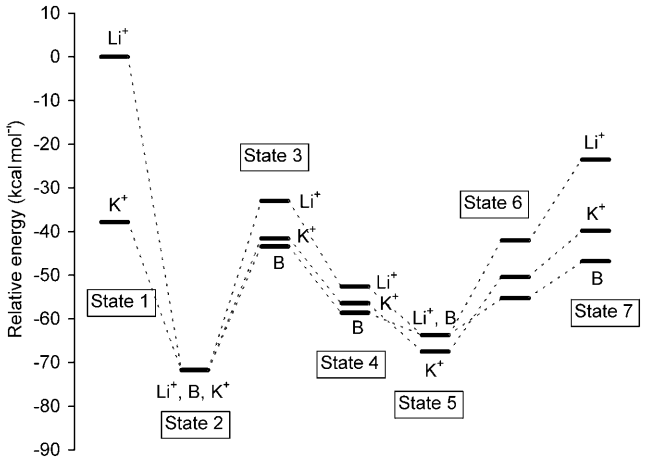

Figure 9. Energy profiles of the metathesis reactions of $\mathbf{1}\cdot Li^+$, $\mathbf{1}\cdot K^+$ and **1** with ethene (**B** represents the bare complexes without Li^+ or K^+). State 1: uncoordinated **1** and M^+ ($M^+ = Li^+$ or K^+); State 2: adduct ions $\mathbf{1}\cdot M^+$ and **1**; State 3: monophosphine complexes $\mathbf{1a}\cdot M^+$ and **1a**; State 4: first π-complex [$\mathbf{1a}\cdot M^+$(**1a**)+ethene]; State 5: Ru cyclobutane intermediates; **State 6**: second π-complex [$\mathbf{4a}\cdot M^+$(**4a**)+styrene]; State 7: products of metathesis reactions: $\mathbf{4a}\cdot M^+$(**4a**)+styrene.

*The coordination of Li^+ or K^+ with **1***: Figure 8 shows the structures of $\mathbf{1}\cdot Li^+$ and $\mathbf{1}\cdot K^+$, in which the Li^+ or K^+ is attached to Cl(2) of catalyst **1**. The angle of Ru-Cl(2)-Li^+ is 68.8° and the angle of Ru-Cl(2)-K^+ is 120.7 °. The interaction energy of catalyst **1** with Li^+ is 71.7 kcal mol^{-1} and with K^+ is even higher, 33.9 kcal mol^{-1}. The cationization increased the Ru–phosphine dissociation energy from 28.3 kcal mol^{-1} for **1** to 30.1 kcal mol^{-1} for $\mathbf{1}\cdot K^+$ and 38.7 kcal mol^{-1} for $\mathbf{1}\cdot Li^+$. The calculated phosphine dissociation energy of **1** is in reasonable agreement with the experimental value of 23.6 ± 0.5 kcal mol^{-1},[19] and the most recently reported value of 33.4 ± 2.3 kcal mol^{-1},[26] and with reported computational results between 21.1[17c] and 24.9,[17d] and up to > 30 kcal mol^{-1}.[27]

Table 2. Change of energy along the metathesis reaction coordinate [kcal mol^{-1}].

Reaction channels	Bare	$M^+ = Li^+$	$M^+ = K^+$
$M^+ + \mathbf{1} \rightarrow \mathbf{1}\cdot M^+$	–	−71.7	−33.9
$\mathbf{1}\cdot M^+ \rightarrow \mathbf{1a}\cdot M^+ + PCy_3$	28.3	38.7	30.1
$\mathbf{1}\cdot M^+ \rightarrow [\mathbf{1}-Cl]^+ + MCl$	–	32.3	31.5
$\mathbf{1a}\cdot M^+ + CH_2{=}CH_2 \rightarrow$ first π complex	−15.2	−19.6	−14.8
first π complex → Ru–cyclobutane	−5.1	−11.1	−11.1
Ru–cyclobutane → second π complex	8.5	21.7	17.1
second π complex → $\mathbf{4a}\cdot M^+ + CH_2{=}CHPh$	8.4	18.5	10.6

In **1**, $\mathbf{1}\cdot Li^+$ and $\mathbf{1}\cdot K^+$, the length of the Ru–Cl(2) bond was found to be 2.458, 2.521 and 2.519 Å, respectively. The changes in the Ru–Cl(2) bond indicated that the coordination of **1** with Li^+ or K^+ weakened the Ru–Cl(2) bond. The Ru–Cl(2) dissociation energy of $\mathbf{1}\cdot Li^+$ to give $[\mathbf{1}-Cl]^+$ and LiCl is 32.3 kcal mol^{-1} and the respective dissociation energy of $\mathbf{1}\cdot K^+$ is 31.5 kcal mol^{-1}.

*Molecular orbital analysis of **1a**, $\mathbf{1a}\cdot Li^+$ and $\mathbf{1a}\cdot K^+$*: The orientation of ethene in the first π complex can be rationalized by the HOMO topology of the Ru complex and the LUMO topology of ethene.[18] The HOMO is localized at the C-Ru-Cl moiety, with small contributions from the phosphine ligand. In order to obtain maximum orbital overlap in the course of the reaction, the C=C axis should be parallel to the Cl-Ru-Cl moiety, when the C=C double bond approaches to the Ru center. The shapes of the HOMO and LUMO of the monophosphine Ru complex **1a** are similar to those of $\mathbf{1a}\cdot Li^+$ and $\mathbf{1a}\cdot K^+$.

Because we did not calculate the structures and energies of the transition states from state 4 to state 5 and from state 5 to state 6, we cannot compare the reaction rates of **1a**, $\mathbf{1a}\cdot Li^+$ and $\mathbf{1a}\cdot K^+$ with ethene. However, we can compare the relative energies of the corresponding intermediates on the reaction coordinate of **1a**, $\mathbf{1a}\cdot Li^+$ or $\mathbf{1a}\cdot K^+$ and ethene. Table 2 and Figure 9 show, in comparison with the bare complex **1**, that the energy profiles along the reaction coordinate of the Li^+ adduct ions and K^+ adduct ions were changed to a different extent. Li^+ addition increased the binding energy with phosphine, which caused the slow initiation of precatalyst $\mathbf{1}\cdot Li^+$ to give the catalytically active species $\mathbf{1a}\cdot Li^+$. Furthermore Li^+ addition also increased the binding energy with olefins in both first and second π complexes, thus increasing the dissociation energy of the second π complex (state 6) to give the products. In summary, it can

be expected that Li^+ cationization of Ru complex **1** will reduce the metathesis reactivity. In contrast, the energy profile of the reaction of **1**·K^+ is much more similar to the bare Ru complex **1**, which is in good agreement with our experimental results. **1a**·K^+ gave **4a**·K^+ in the gas phase reaction of **1a**·K^+ with ethene; however, we did not observe **4a**·Li^+ in the gas phase reaction of **1a**·Li^+ with ethene.

Discussion

Our results clearly demonstrate that the Ru complex **1** can be cationized with alkali metal ions and that the cationized Ru species can be detected using ESIMS with high sensitivity. The alkali-metal cation is coordinated to a chloride ligand as shown by our MS/MS results and theoretical calculations. We were able to detect the expected Ru species present in solution, including the catalytically active monophosphine complex (Scheme 2), which confirms our recently reported results.[10] The MS/MS spectra for the CID of the ions **1**·M^+ showed that the coordinated cation M^+ has a strong influence on the fragmentation behavior (Figure 1). Remarkably, the strong binding energy of Li^+ (71.7 kcal mol^{-1}) or K^+ (33.9 kcal mol^{-1}) with **1** had the effect that the CID give useful fragmentations of the respective ions and not only splitting of the alkali cation. It has already been demonstrated for cationized fatty alcohols[12d,e] that alkali-metal cations can be attached to a polar functional group and decompositions can be induced to occur independent of the charge and remote from the charge site. With increasing Lewis acidity of M^+ going from Cs^+ to K^+ to Na^+ and to Li^+, the ratio of the elimination of Cy_3P and of MCl in MS/MS is reduced by about two orders of magnitude corresponding to increasing Ru–phosphine and much less increasing Ru–Cl bond dissociation energy (Table 2). In the MS/MS of **1**·Li^+ at *m/z* 829 (Figure 1a), the intensity of $[\mathbf{1}-Cl]^+$ at *m/z* 787 was much higher than that of **1a**·Li^+ at *m/z* 549 due to the Ru–Cl dissociation energy (32.3 kcal mol^{-1}) being 6.4 kcal mol^{-1} lower than the Ru–phosphine dissociation energy (38.7 kcal mol^{-1}) of **1**·Li^+. However, in the MS/MS of **1**·K^+ at *m/z* 861 (Figure 1c), the intensity of **1a**·K^+ at *m/z* 581 was higher than that of $[\mathbf{1}-Cl]^+$ at *m/z* 787 due to the Ru–phosphine dissociation energy of 30.1 kcal mol^{-1} being 1.4 kcal mol^{-1} lower than the Ru–Cl dissociation energy (31.5 kcal mol^{-1}) of **1**·K^+.

A significant effect of the Lewis acidity can also be observed comparing the MS/MS spectra of the 14-electron intermediates **1a**·M^+. Thus, the ratio of the elimination of ($C_7H_8 + H_2$) and of C_7H_8 increases with increasing Lewis acidity of the alkali cation. (Figure 2). The observed preferential scission of the benzylidene unit of **1a**·M^+ using only low collision energy (2 eV) in contrast to the bisphosphine ion **1**·M^+ (collision energy 8–10 eV) provides evidence that, in going from **1** to **1a**, new, low-energy reaction channels may be opened with participation of the phosphine ligand providing the hydrogen atoms needed for the observed eliminations through a possible C–H bond activation by the coordinatively unsaturated Ru center. The fragmentation of the carbene ligands as an important dissociation pathway of the 14-electron Ru complexes has been reported,[10] and the following dehydrogenation phenomenon has been widely observed in MS/MS spectra of other organic metal complexes[28] through the C–H activation mechanism.[29]

It can be expected that the Lewis acidity of the alkali cation will also influence the metathesis activity. Evidently, the concentration of the catalytically active 14-electron species will be reduced with increasing Lewis acidity going from Cs^+ to K^+ to Na^+ and to Li^+ by approximately one order of magnitude (Table 1). The most important question is whether the catalytic activity is retained in the presence of alkali halides and whether cationized **1a** is catalytically active. The gas-phase ion–molecule reactions performed with 1-butene and ethene give unambiguous evidence for the intrinsic catalytic activity of **1a**·K^+ (Figure 3, Scheme 3). Interestingly, as expected, the catalytic activity of **1a**·K^+ is significantly higher than that of **1a**·Li^+ because of the higher Lewis acidity of Li^+. A metathesis reaction was observed with both ions and 1-butene. The **1a**·K^+ species also catalyzed the reaction with ethene in contrast to **1a**·Li^+. This experimental result is in agreement with our quantum-mechanical calculations. The reaction of **1a**·Li^+ and ethene to give **4a**·Li^+ and styrene was found to be endothermic by 9.5 kcal mol^{-1}, whereas the respective reaction of **1a**·K^+ was found to be endothermic by only 1.8 kcal mol^{-1} (Figure 9, Table 2).

We could not find any experimental evidence for a Ru–alkene π complex or a ruthenacyclobutane, which are generally accepted as intermediates of the metathesis catalytic cycle (Scheme 1), neither in the gas phase nor in liquid phase and could confirm these earlier results.[6,7,10] Adlhart et al. showed by quantum-chemical calculations that the rate determining transition state may have ruthenacylobutane structure, although alternative explanations cannot be wholly ruled out.[7b,17c]

Most interestingly, the ion $[\mathbf{1a}-Cl]^+$ proved to be able to coordinate ethene, but not to catalyze the metathesis reaction.[18] The calculations revealed that the HOMO of **1a**, which is responsible for the formation of the π complex, is localized mainly at the Cl-Ru-Cl moiety and is dramatically changed in the complex $[\mathbf{1a}-Cl]^+$. Evidently, both chloride ligands are necessary for the catalytic activity.

Using the tool of cationization, we studied the RCM reactions of α,ω-dienes **5–7** with catalyst **1** and could unambiguously detect and characterize the K^+ adduct ions of alkylidene intermediates of the catalytic cycle **8–10** and **8a–10a**, as well. This is most remarkable because we were unable to detect the respective intermediates using a charge-labeled phosphine to study the reaction by mass spectrometry.[10] Evidently, the cationization slowed down the rate of the intramolecular metathesis reaction of **8a–10a** to give the final RCM products. Recently, P′Pool and Schanz tried to observe the alkylidene Ru intermediates in the RCM reaction of dienes by NMR spectroscopy, but no conclusive results were obtained.[11b] Interestingly, the ratio of the intensities of the

respective ions of intermediates **8a**·K^+–**10a**·K^+ and **8**·K^+–**10**·K^+ was found to be about one order of magnitude higher than the ratio of **1a**·K^+ and **1**·K^+ (Table 1). This can be explained by the intramolecular coordination of the ω-double bond of the alkylidene to the Ru atom in competition with the intermolecular coordination of tricyclohexylphosphine.[9,23,24] Moreover, the K^+ adduct ions **8a**–**10a** showed a smooth intramolecular metathesis reaction in the gas phase and elimination of the respective cycloalkenes **11**–**13**. Thus, we performed the first catalytic step of RCM in the liquid phase, transferred the intermediates **8a**·K^+–**10a**·K^+ in the gas phase and observed the second step of the RCM cycle. Adlhart et al. reported a special example of a gas phase RCM reaction.[7]

1,9-Decadiene (**14**) showed, as expected, ADMET polymerization instead of RCM.[21,22] Cationization with K^+ enabled easy detection of the monophosphine–alkylidene intermediates **15a**, the first intermediate of the ADMET catalytic cycle, and **16a** and **17a**, the next higher intermediates in the catalytic cycle, respectively, as well as the methylidene–Ru intermediate **4a**. RCM with elimination of cyclooctene was observed in the gas phase using MS/MS for the CID of **15a**·K^+ with a very low collision energy (Figure 5a). The rate of elimination of cyclooctene is slower by approximately one order of magnitude compared with the respective elimination of cyclohexene (Figure 4b). Thus, RCM of 1,9-decadiene (**14**) may also be possible in solution using proper conditions under high dilution.[21] The respective K^+ adduct ions of the bisphosphine products **15**, **16**, **17** as well as **4**, formed in the equilibrium with free phosphine, were observed as well. The ratio of the intensities of monophosphine **15a**·K^+, **16a**·K^+ and **17a**·K^+ to bisphosphine intermediates **15**·K^+, **16**·K^+ and **17**·K^+, respectively, was found to be about 0.2–0.5, one order of magnitude higher than that of the respective ratio of **4a** and **4** (Table 1), which gives evidence for intramolecular coordination of C=C bonds of the alkylidene chain to Ru.

All alkylidene intermediates **19a**–**21a** and **19**–**21** were also easily detected as K^+ adduct ions and characterized directly from the reaction solution of the ROMP of cyclooctene (**18**, Scheme 6). MS/MS for the CID of **19a**·K^+–**21a**·K^+ showed, similarly to that already discussed for ADMET, a "retro-ROMP," that is RCM to eliminate cyclooctene and cyclooctene oligomers, respectively, giving the primary benzylidene catalyst **1a**·K^+ (Figure 6). Adlhart et al. studied the ROMP of norbornene by ESIMS using catalyst **1** and reported that subsequent to initiation, the catalytic cycle proceeds through the monophosphine complex without further significant involvement of a bisphosphine complex, in other words, the resting state of the catalyst in ROMP is the monophosphine complex as opposed to the bisphosphine resting state in acyclic olefin metathesis.[9] Probably, this observation is a special result limited to norbornene. Our results give evidence that in all of the metathesis reactions studied using the first-generation catalyst **1**, significant involvement of a bisphosphine complex can be observed even in the special case of the reaction of 1,5-hexadiene (**22**). The metathesis intermediate **23a** is extremely stabilized by the ω-double bond.[22,23] However, in equilibrium with the Cy_3P present in solution, the bisphosphine complex **23** is also formed. The ratio of the intensities of **23a**·K^+ and **23**·K^+ was about 10 (Table 1). In all examples studied, we observed a stabilization of the monophosphine complex by double bonds in the alkylidene chain. However, the bisphosphine complex was, in general, the major compound with one further exception. The ratio of the intensities of **19a**·K^+ and **19**·K^+, the first intermediate of ROMP of cyclooctene, was 2.1. This extremely high stabilization of the monophosphine complex **19a** compared to the homologues **20a** and **21a** may possibly be explained by a stronger donor ability of the styryl group compared to an aliphatic double bond to Ru (Table 1).[7a]

Conclusion

In conclusion, it was shown that cationization of the neutral first-generation ruthenium olefin metathesis catalyst **1** by simple addition of alkali chlorides to the reaction solution allowed the mass spectrometric study of **1** by ESIMS and, most importantly, of intermediates in the catalytic cycle of RCM, ADMET, ROMP, and other reactions in solution. It was possible for the first time to detect and to characterize, in all of the reactions studied, the monophosphine–Ru intermediates of the catalytic cycle directly from solution. The unambiguous detection of the alkylidene–Ru intermediates of RCM directly from the on-going reaction solution seems to be of particular importance as well as the possibility to quantify intramolecular π-complex formation by measurement of the ratio of the intensities of the mono- and respective bisphosphine–Ru intermediate, which can be obtained easily from a simple ESI spectrum. Moreover, the catalytic activity of the alkylidene–Ru intermediates of RCM completing the catalytic cycle by elimination of the respective cycloalkene and formation of the methylidene–Ru complex was easily shown in the gas phase. This simple tool of cationization of neutral Ru complexes to enable their mass spectrometric investigation, which has not been used up to now, is not restricted to first-generation catalysts and may be applied more generally, particularly to second-generation and Hoveyda–Grubbs Ru catalysts.

Experimental Section

General Remarks: CH_2Cl_2, anhydrous CH_3OH, Ru catalysts **1** and **2**, alkali metal chloride salts LiCl, NaCl, KCl, and CsCl, 1,6-heptadiene (**5**), 1,7-octadiene (**6**), 1,8-nonadiene (**7**), 1,9-decadiene (**14**), cyclooctene (**18**), and 1,5-hexadiene (**22**) were purchased from Aldrich (Steinheim, Germany) and used as received. All reactions were performed at room temperature. The solvent, CH_2Cl_2, was dried by distillation over CaH_2 as the drying agent prior to use. CH_3OH and CH_2Cl_2 were saturated with argon before use.

ESIMS experimental conditions: The mass spectrometric measurements were performed on a Micromass Premier quadrupole-time of flight (Q-

TOF) instrument (Waters, Manchester) equipped with an ESI ion source containing a stainless steel metal spray capillary (127 μm inner diameter, 229 μm outer diameter, 181 mm of length). The capillary voltage (3.5 kV) source and desolvation temperature of 50 °C and cone voltage of 20 eV were applied as standard ESI operating conditions. The collision induced dissociation (CID, collision gas argon with flow rate at 0.2 mL min^{-1}) was performed in the collision cell region; the collision energy varied depending on ion species studied.

General procedures for the on-line microreactor ESIMS study of the alkali-metal-cationized Ru catalyst 1: A solution of **1** (0.4 mg, 5.5×10^{-5} M) in CH_2Cl_2 (10 mL) was prepared and mixed with a solution of LiCl (0.1 mg, 2.4×10^{-4} M) in CH_3OH (10 mL) using two respective syringes feeding a microreactor (Techlab, Peek mixing tee) coupled directly to the ESIMS ion source. The injection speed of both solutions was settled at 5 μL min^{-1}, which allowed the study of the solution after a reaction time of approximately 12 s. Catalyst **1** cationized by Na^+, K^+, or Cs^+ could be studied by using solutions of NaCl, KCl, or CsCl in CH_3OH in similar concentration.

General procedures for the on-line microreactor ESIMS study of the olefin metathesis reactions of catalyst 1 with dienes 5, 6, 7, 14, 22 or 18 in the presence of KCl: An aliquot of a solution of **5**, **6**, **7**, **14**, **22** or **18** (1 mg, 1.0×10^{-3} M) in CH_3OH (10 mL) in the presence of KCl (0.2 mg, 2.7×10^{-4} M) was mixed with an aliquot of a solution of **1** (0.4 mg, 5.5×10^{-5} M) in CH_2Cl_2 (10 mL) by using two respective syringes feeding a mixing tee coupled directly to the ESIMS ion source. The injection speed of both solutions was settled at 5 μL min^{-1}, which allowed the study of the reaction after a reaction time of 12 s.

ADMET polymerization of 1,9-decadiene (14): 1,9-Decadiene (**14**, 1.5 mg, 1.1×10^{-3} M) and **1** (0.4 mg, 5.5×10^{-5} M) were dissolved in CH_2Cl_2 (10 mL). After a reaction time of 1 h with agitation, an aliquot of this reaction solution was mixed with an aliquot of a solution of KCl (0.2 mg, 2.7×10^{-4} M) in CH_3OH (10 mL) by using two respective syringes with an injection speed of 5 μL min^{-1} feeding a mixing tee coupled directly to the ESIMS ion source.

Gas-phase metathesis reaction of Li^+ or K^+ adduct ions of 1 and 1a with 1-butene and ethene, respectively: The collision cell of the Q-TOF was filled with 1-butene (Aldrich, Steinheim, Germany). The 1-butene pressure was maintained approximately at 2.0×10^{-3} mbar. The monoisotopic Li^+ or K^+ adduct ion of **1** and **1a**, respectively, was selected in the first quadrupole to react with 1-butene in the collision cell under low-energy collisions (0.5–2.0 eV), and the product ions were detected by the TOF analyzer. The respective experiments were performed with ethene. The ion $[\mathbf{1a}-Cl]^+$ was reacted analogously with ethene.

Computations: First, we used a simplified model, in which the PCy_3 ligand was replaced by $P(CH_3)_3$. Then, we used the Vienna ab initio Simulation Package (VASP)[31] and Gaussian 03 software package to perform density functional theory (DFT) calculations.[32] The Perdew–Burke–Ernzerhof (PBE) exchange-correlation functional within generalized gradient approximation (GGA) was chosen.[33] The simplified model structures were thermally annealed at 300 K using the Nosé thermostat implemented in VASP.[34]

The model structures were pre-optimized by VASP without dipole correction. Based on the pre-optimized structures, geometry optimizations using tighter convergence criteria were undertaken using Gaussian 03. In VASP calculations, pseudopotentials constructed by the projector augmented wave (PAW) method were adopted.[31] The planewave energy cutoff was set to 300 eV and 400 eV for molecular dynamics and geometry optimizations, respectively. The energy cutoff for the augmentation charge density was set to 645 eV. In Gaussian 03 calculations, geometry optimizations were carried out at the PBEPBE/6–31G* level of theory, and the single point energy was calculated at PBEPBE/6–311+G (2d,p) level of theory. For Ru, a Los Alamos National Laboratory 2-double-z (LANL2DZ) basis set with effective core potential was adopted.

Acknowledgements

Financial support from German Research Association (DFG) is gratefully acknowledged by H.-Y.W. and J.O.M. (Me 722/18). W.-L.Y. and T.K. thank the Alexander-von-Humboldt Foundation and the Hanse Institute for Advanced Study for support. H.-Y.W. thanks the support from National Natural Science Foundation of China (20942002).

[1] Reviews: a) R. H. Grubbs, S. Chang, *Tetrahedron* **1998**, *54*, 4413–4450; b) T. M. Trnka, R. H. Grubbs, *Acc. Chem. Res.* **2001**, *34*, 18–29; c) R. H. Grubbs, *Tetrahedron* **2004**, *60*, 7117–7140; d) A. Fürstner, *Angew. Chem.* **2000**, *112*, 3140–3172; *Angew. Chem. Int. Ed.* **2000**, *39*, 3012–3043.

[2] *Handbook of Metathesis, Vols. 1–3* (Ed.: R. H. Grubbs), Wiley-VCH, Weinheim, Germany, **2003**.

[3] a) L. S. Santos, L. Knaack, J. O. Metzger, *Int. J. Mass Spectrom.* **2005**, *246*, 84–104; b) M. N. Eberlin, *Eur. J. Mass Spectrom.* **2007**, *13*, 19–28; c) L. S. Santos, *Eur. J. Org. Chem.* **2008**, 235–253.

[4] a) S. Meyer, J. O. Metzger, *Anal. Bioanal. Chem.* **2003**, *377*, 1108–1114; b) S. Fürmeier, J. O. Metzger, *J. Am. Chem. Soc.* **2004**, *126*, 14485- 14492; c) L. S. Santos, C. H. Pavam, W. P. Almeida, F. Coelhoand, M. N. Eberlin, *Angew. Chem.* **2004**, *116*, 4430–4433; *Angew. Chem. Int. Ed.* **2004**, *43*, 4330–4333; d) X. Zhang, Y. Liao, R. Qian, H. Wang, Y. Guo, *Org. Lett.* **2005**, *7*, 3877–3880; e) C. Marquez, J. O. Metzger, *Chem. Commun.* **2006**, 1539–1541; f) J. Roithová, D. Schröder, *Chem. Eur. J.* **2008**, *14*, 2180–2188.

[5] a) A. A. Sabino, A. H. L. Machado, C. R. D. Correia, M. N. Eberlin, *Angew. Chem.* **2004**, *116*, 2568; *Angew. Chem. Int. Ed.* **2004**, *43*, 2514-.2518; b) L. S. Santos, J. O. Metzger, *Angew. Chem.* **2006**, *118*, 991–995; *Angew. Chem. Int. Ed.* **2006**, *45*, 977–981; c) L. S. Santos, G. B. Rosso, R. A. Pilli, M. N. Eberlin, *J. Org. Chem.* **2007**, *72*, 5809–5812; d) J. Comelles, A. Pericas, M. Moreno-Mañas, A. Vallribera, G. Drudis-Solé, A. Lledos, T. Parella, A. Roglans, S. García-Granda, L. Roces-Fernández, *J. Org. Chem.* **2007**, *72*, 2077–2087; e) L. S. Santos, J. O. Metzger, *Rapid Commun. Mass Spectrom.* **2008**, *22*, 898–904.

[6] a) C. Hinderling, C. Adlhart, P. Chen, *Angew. Chem.* **1998**, *110*, 2831–2835; *Angew. Chem. Int. Ed.* **1998**, *37*, 2685–2689; b) P. Chen, *Angew. Chem.* **2003**, *115*, 2938–2954; *Angew. Chem. Int. Ed.* **2003**, *42*, 2832–2847.

[7] C. Adlhart, C. Hinderling, H. Baumann, P. Chen, *J. Am. Chem. Soc.* **2000**, *122*, 8204–8214.

[8] a) B. Mohr, D. M. Lynn, R. H. Grubbs, *Organometallics* **1996**, *15*, 4317–4325; b) T. A. Kirkland, D. M. Lynn, R. H. Grubbs, *J. Org. Chem.* **1998**, *63*, 9904–9909.

[9] C. Adlhart, P. Chen, *Helv. Chim. Acta* **2000**, *83*, 2192–2196.

[10] H.-Y. Wang, J. O. Metzger, *Organometallics* **2008**, *27*, 2761–2766.

[11] a) C. W. Bielawski, R. H. Grubbs, *Macromolecules* **2001**, *34*, 8838–8840; b) S. J. P′Pool, H.-J. Schanz, *J. Am. Chem. Soc.* **2007**, *129*, 14200–14212.

[12] a) T. Fujii, *Mass Spectrom. Rev.* **2000**, *19*, 111–138; b) G. E. Hofmeister, Z. Zhou, J. A. Leary, *J. Am. Chem. Soc.* **1991**, *113*, 5964–5970; c) H.-Y. Wang, Y.-L. Guo, L. Lu, *J. Am. Soc. Mass Spectrom.* **2004**, *15*, 1820–1832; d) J. Adams, M. L. Gross, *J. Am. Chem. Soc.* **1986**, *108*, 6915–6921; e) J. Adams, M. L. Gross, *Anal. Chem.* **1987**, *59*, 1576–1582; f) F. L. D′Alexandri, F. C. Gozzo, M. N. Eberlin, A. M. Katzin, *Anal. Biochem.* **2006**, *355*, 189–200.

[13] a) R. Colton, A. D′Agostino, J. C. Traeger, *Mass Spectrom. Rev.* **1995**, *14*, 79–106; b) J. C. Traeger, *Int. J. Mass Spectrom.* **2000**, *200*, 387–401.

[14] G. K. Poon, P. Mistry, S. Lewis, *Biol. Mass Spectrom.* **1991**, *20*, 687–692.

[15] C. Decker, W. Henderson, B. K. Nicholson, *J. Chem. Soc. Dalton Trans.* **1999**, 3507–3513.

[16] M. J. Marsella, H. D. Maynard, R. H. Grubbs, *Angew. Chem.* **1997**, *109*, 1147–1150; *Angew. Chem. Int. Ed. Engl.* **1997**, *36*, 1101–1103.

[17] a) L. Cavallo, *J. Am. Chem. Soc.* **2002**, *124*, 8965–8973; b) S. F. Vyboishchikov, M. Bühl, W. Thiel, *Chem. Eur. J.* **2002**, *8*, 3962–3975;

c) C. Adlhart, P. Chen, *J. Am. Chem. Soc.* **2004**, *126*, 3496–3510; d) C. Adlhart, P. Chen, *Handbook of Metathesis, Vol. 1* (Ed.: R. H. Grubbs), Wiley-VCH, Weinheim, **2003**, pp. 132–172; e) M. Piacenza, I. Hyla-Kryspin, S. Grimme, *J. Comput. Chem.* **2007**, *28*, 2275–2285.

[18] See the Supporting Information.

[19] a) M. S. Sanford, M. Ulman, R. H. Grubbs, *J. Am. Chem. Soc.* **2001**, *123*, 749–750; b) M. S. Sanford, J. A. Love, R. H. Grubbs, *J. Am. Chem. Soc.* **2001**, *123*, 6543–6554.

[20] a) G. C. Fu, S. T. Nguyen, R. H. Grubbs, *J. Am. Chem. Soc.* **1993**, *115*, 9856–9857; b) R. H. Grubbs, S. J. Miller, ; G. C. Fu, *Acc. Chem. Res.* **1995**, *28*, 446–452; G. C. Fu, *Acc. Chem. Res.* **1995**, *28*, 446–452; c) T. A. Kirkland, R. H. Grubbs, *J. Org. Chem.* **1997**, *62*, 7310–7318; d) M. L. Ferguson, D. J. O'Leary, R. H. Grubbs, *Org. Synth.* **2003**, *80*, 85–92.

[21] S. E. Lehmann, Jr, K. B. Wagener, *Handbook of Metathesis, Vol. 3* (Ed.: R. H. Grubbs), Wiley-VCH, Weinheim, **2003**, pp. 283–353.

[22] K. Brzezinska, P. S. Wolfe, M. D. Watson, K. B. Wagener, *Macromol. Chem. Phys.* **1996**, *197*, 2065–2074.

[23] a) S. T. Nguyen, L. K. Johnson, R. H. Grubbs, .J. W. Ziller, *J. Am. Chem. Soc.* **1992**, *114*, 3974–3975; b) J. A. Tallarico, P. J. Bonitatebus, Jr., M. L. Snapper, *J. Am. Chem. Soc.* **1997**, *119*, 7157–7158.

[24] K. B. Wagener, K. Brzezinska, J. D. Anderson, T. R. Younkin, K. Steppe, W. DeBoer, *Macromolecules* **1997**, *30*, 7363–7369.

[25] Z. Wu, A. D. Benedicto, R. H. Grubbs, *Macromolecules* **1993**, *26*, 4975–4977.

[26] S. Torker, D. Merki, P. Chen, *J. Am. Chem. Soc.* **2008**, *130*, 4808–4814.

[27] Y. Zhao, D. G. Truhlar, *Org. Lett.* **2007**, *9*, 1967–1970.

[28] a) D. Feichtinger, D. A. Plattner, P. Chen, *J. Am. Chem. Soc.* **1998**, *120*, 7125–7126; b) D. E. Richardson, N. G. Alameddin, M. F. Ryan, T. Hayes, J. R. Eyler, A. R. Siedle, *J. Am. Chem. Soc.* **1996**, *118*, 11244–11253.

[29] a) J. A. Labinger, J. E. Bercaw, *Nature* **2002**, *417*, 507–514; b) F. C. Courchay, J. C. Sworen, I. Ghiviriga, K. A. Abboud, K. B. Wagener, *Organometallics* **2006**, *25*, 6074–6086.

[30] a) M. Ulman, R. H. Grubbs, *J. Org. Chem.* **1999**, *64*, 7202–7207; b) B. Chaudret, R. Poilblanc, *Organometallics* **1985**, *4*, 1722–1726.

[31] a) G. Kresse, D. Joubert, *Phys. Rev. B* **1999**, *59*, 1758–1775; b) G. Kresse, J. Furthmüller, *Comput. Mater. Sci.* **1996**, *6*, 15–50; c) G. Kresse, J. Furthmüller, *Phys. Rev. B* **1996**, *54*, 11169–11186.

[32] Gaussian 03, Revision D.01, M. J. Frisch, G. W. Trucks, H. B. Schlegel, G. E. Scuseria, M. A. Robb, J. R. Cheeseman, J. A. Montgomery, Jr., T. Vreven, K. N. Kudin, J. C. Burant, J. M. Millam, S. S. Iyengar, J. Tomasi, V. Barone, B. Mennucci, M. Cossi, G. Scalmani, N. Rega, G. A. Petersson, H. Nakatsuji, M. Hada, M. Ehara, K. Toyota, R. Fukuda, J. Hasegawa, M. Ishida, T. Nakajima, Y. Honda, O. Kitao, H. Nakai, M. Klene, X. Li, J. E. Knox, H. P.Hratchian, J. B. Cross, V. Bakken, C. Adamo, J. Jaramillo, R. Gomperts, R. E. Stratmann, O. Yazyev, A. J. Austin, R. Cammi, C. Pomelli, J. W. Ochterski, P. Y. Ayala, K. Morokuma, G. A. Voth, P. Salvador, J. J. Dannenberg, V. G. Zakrzewski, S.Dapprich, A. D. Daniels, M. C. Strain, O. Farkas, D. K. Malick, A. D. Rabuck, K. Raghavachari, J. B. Foresman, J. V. Ortiz, Q. Cui, A. G. Baboul, S. Clifford, J. Cioslowski, B. B. Stefanov, G. Liu, A. Liashenko, P. Piskorz, I. Komaromi, R. L. Martin, D. J. Fox, T. Keith, M. A. Al-Laham, C. Y. Peng, A. Nanayakkara, M. Challacombe, P. M. W. Gill, B. Johnson, W. Chen, M. W. Wong, C. Gonzalez, J. A. Pople, Gaussian, Inc., Wallingford CT, **2004**.

[33] a) J. P. Perdew, K. Burke, M. Ernzerhof, *Phys. Rev. Lett.* **1997**, *78*, 1396–1396; b) J. P. Perdew, K. Burke, M. Ernzerhof, *Phys. Rev. Lett.* **1996**, *77*, 3865–3868.

[34] a) S. Nosé, *Mol. Phys.* **1984**, *52*, 255–268; b) S. Nosé, *J. Chem. Phys.* **1984**, *81*, 511–519.

Received: March 3, 2009
Published online: September 16, 2009

CHEMISTRY
A EUROPEAN JOURNAL

Supporting Information

ESI-MS Studies and Calculations on Alkali Metal Adduct Ions of Ruthenium Olefin Metathesis Catalysts and Their Catalytic Activities in Metathesis Reactions

Hao-Yang Wang,[a,c] Wai-Leung Yim,[b, d] Thorsten Klüner,[b] and Jürgen O. Metzger*[a]

Institute of Pure and Applied Chemistry, [a] Organic Chemistry, [b] Theoretical Chemistry, Carl von Ossietzky University of Oldenburg, Carl-von-Ossietzky-Str. 9-11, 26129 Oldenburg, Germany

[c]Shanghai Mass Spectrometry Center, Shanghai Institute of Organic Chemistry, Lingling Road 345, Shanghai 200032, China.

[d]Institute of High Performance Computing, 1 Fusionopolis Way, #16-16 Connexis, Singapore 138632, Singapore

1. ESI MS spectra of alkali metal adduct ions of 1.

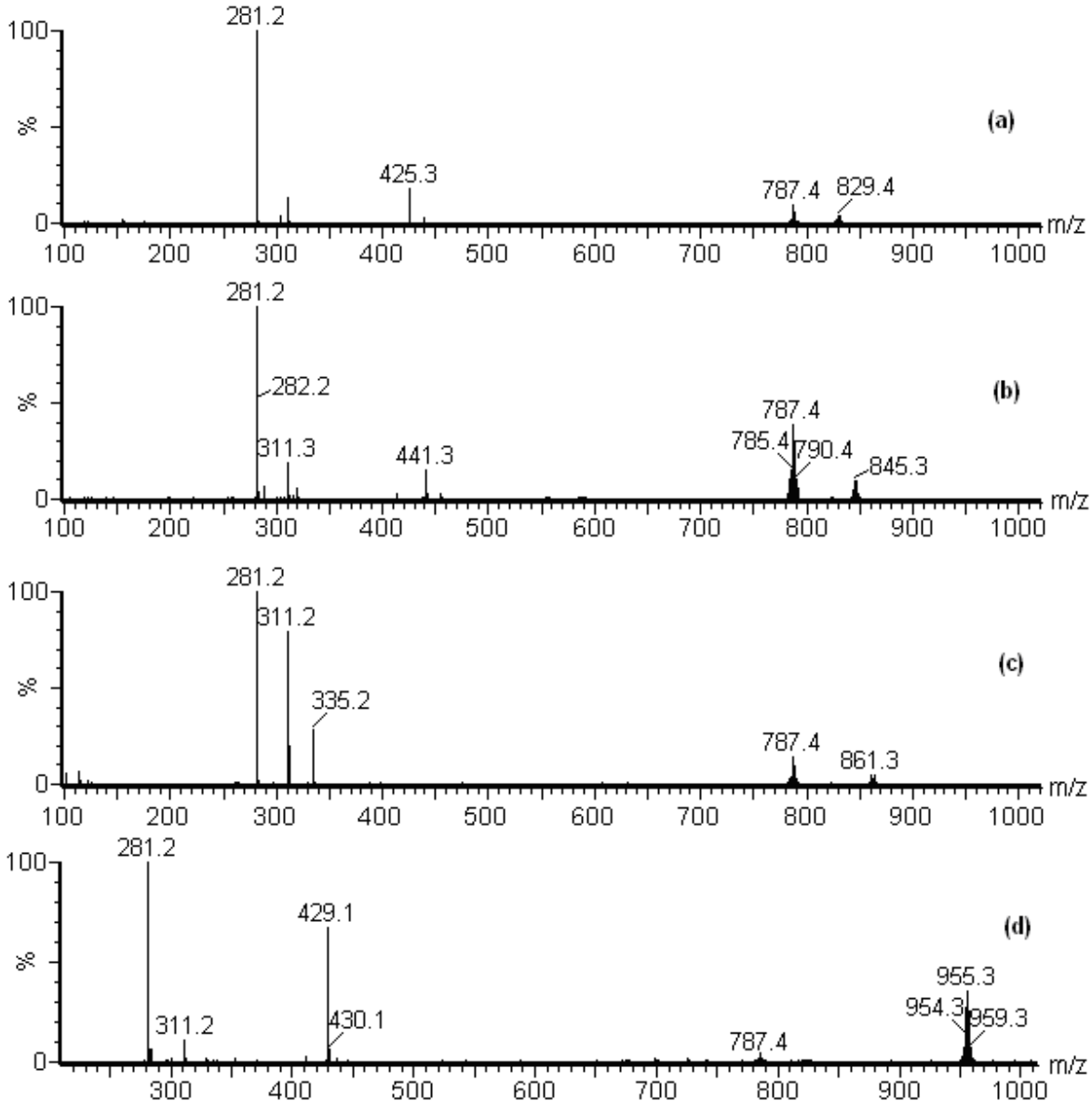

Figure S1. ESI mass spectra obtained by mixing the CH_3OH solution of alkali metal salt with the CH_2Cl_2 solution of **1** using a micro-reactor, coupled on-line to the ESI ion source: (a) LiCl; (b) NaCl; (c) KCl; (d) CsCl, (because Cs^+ at *m/z* 132.9 was in excess, this spectrum was given from *m/z* 150).

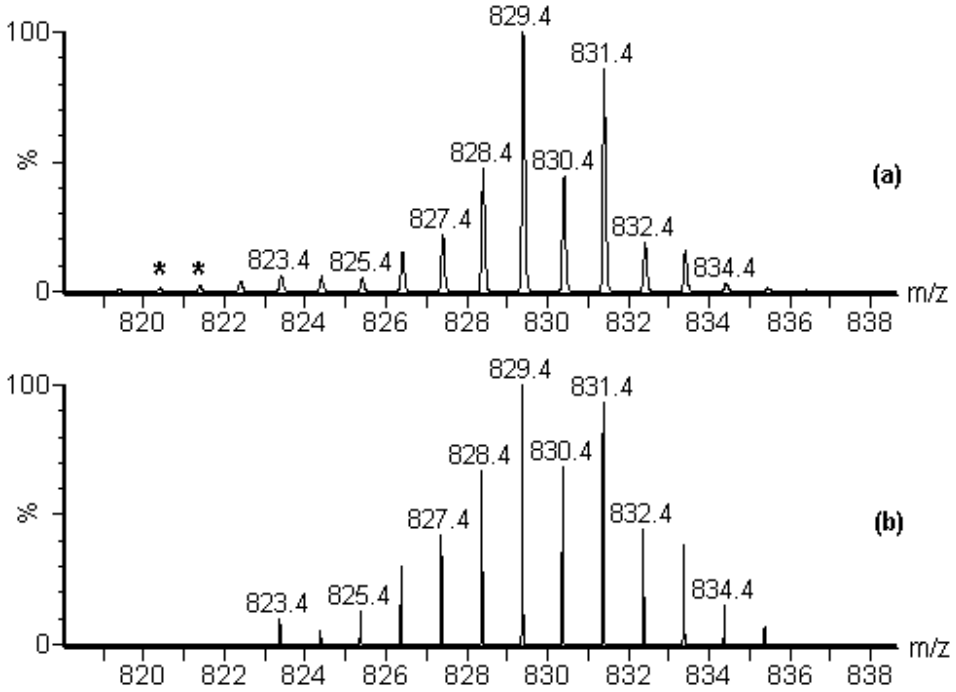

Figure S2. (a) Isotopic pattern of **1**·Li^+; (b) theoretical isotopic pattern of **1**·Li^+. $\mathbf{1}^{\bullet+}$ at *m/z* 822 (marked with "*").

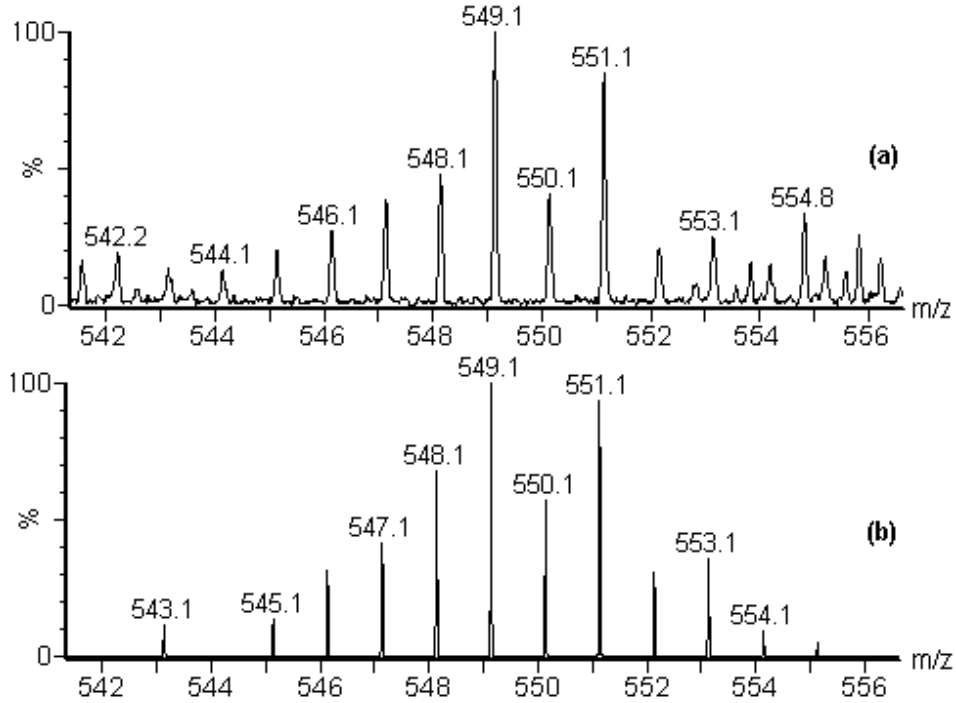

Figure S3. (a) Isotopic pattern of **1a**·Li^+; (b) theoretical isotopic pattern of **1a**·Li^+.

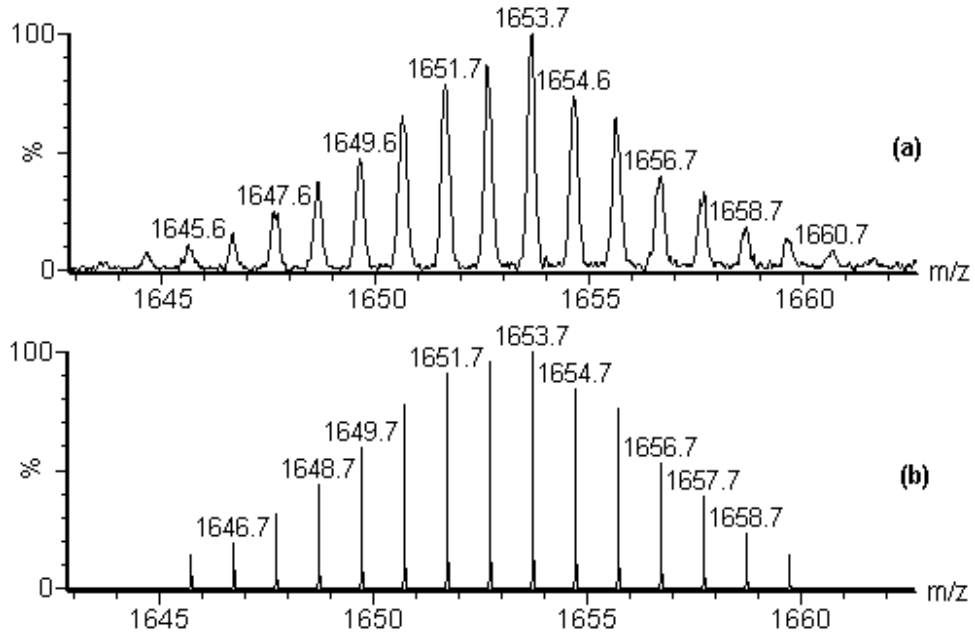

Figure S4. (a) Isotopic pattern of $\mathbf{1}_2 \cdot Li^+$; (b) theoretical isotopic pattern of $\mathbf{1}_2 \cdot Li^+$.

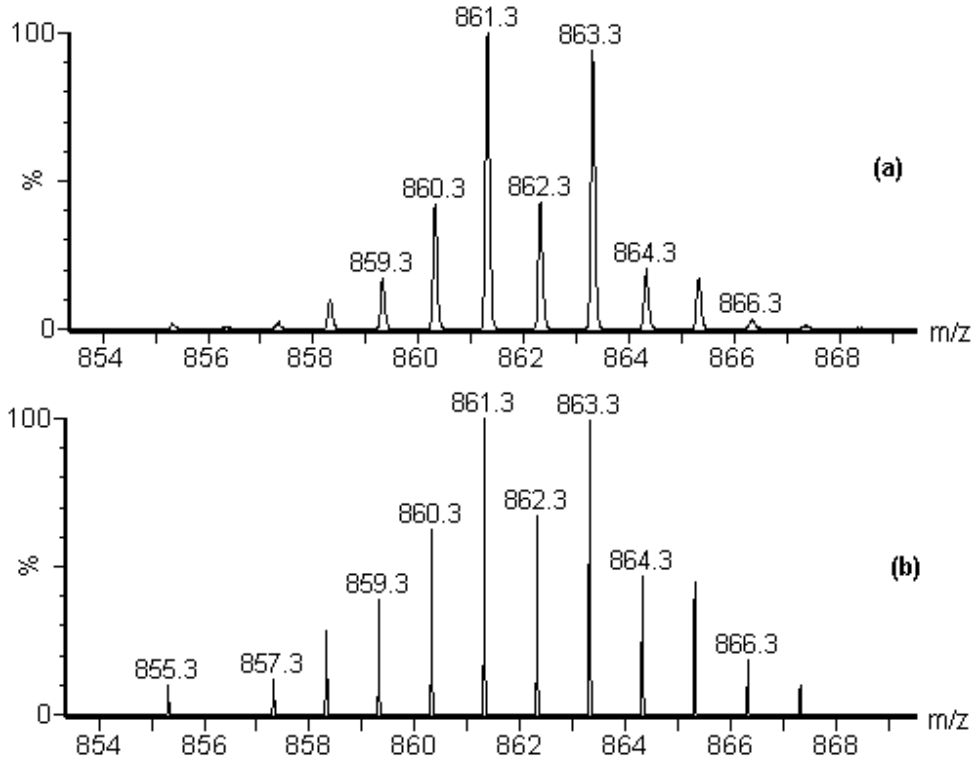

Figure S5. (a) Isotopic pattern of $\mathbf{1} \cdot K^+$; (b) theoretical isotopic pattern of $\mathbf{1} \cdot K^+$.

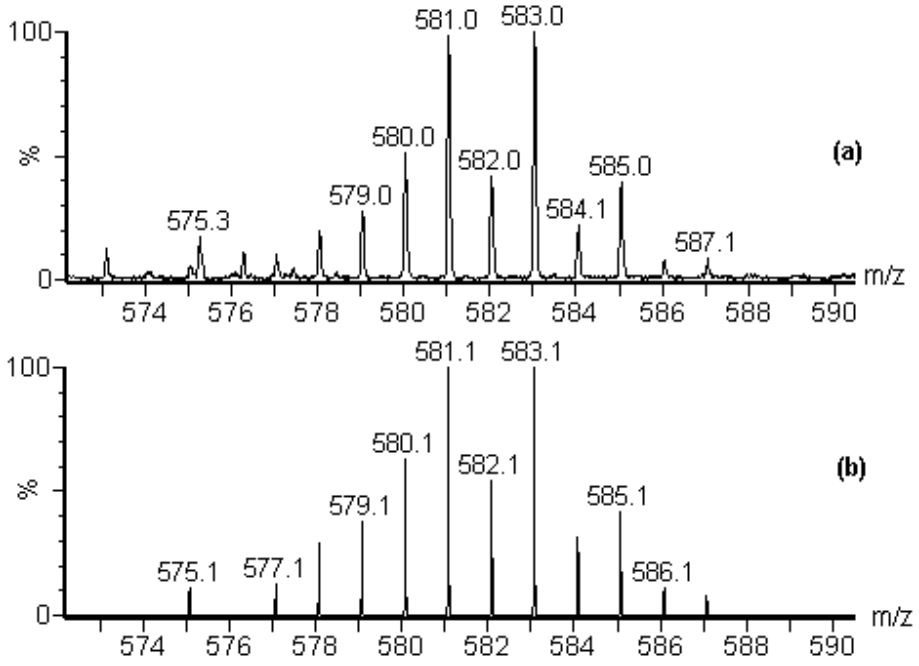

Figure S6. (a) Isotopic pattern of **1a**·K^+; (b) theoretical isotopic pattern of **1a**·K^+.

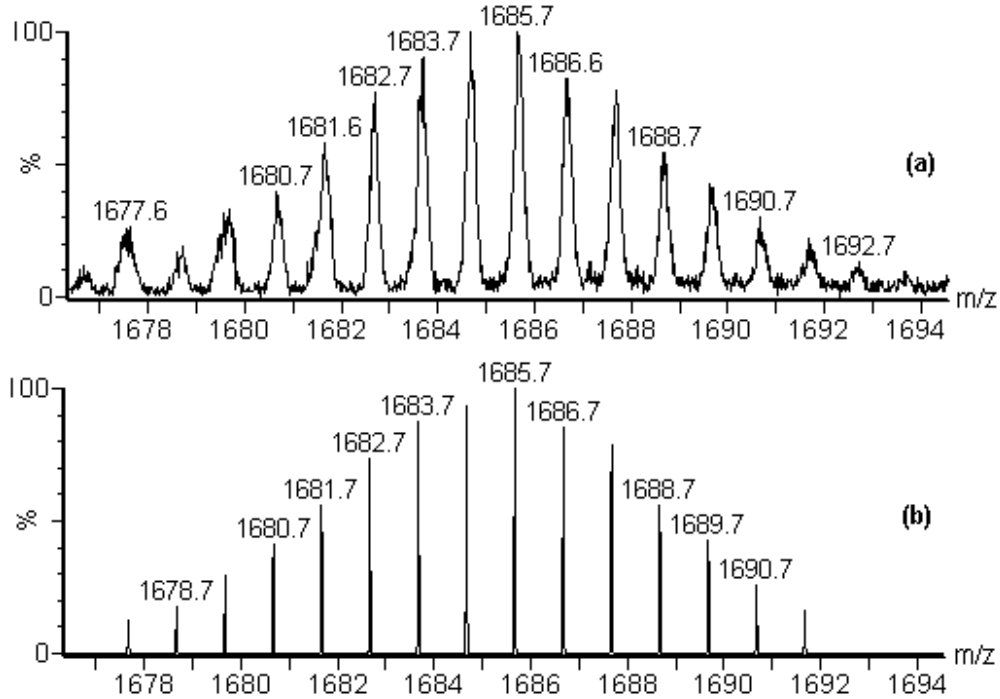

Figure S7. (a) Isotopic pattern of $\mathbf{1}_2$·K^+; (b) theoretical isotopic pattern of $\mathbf{1}_2$·K^+.

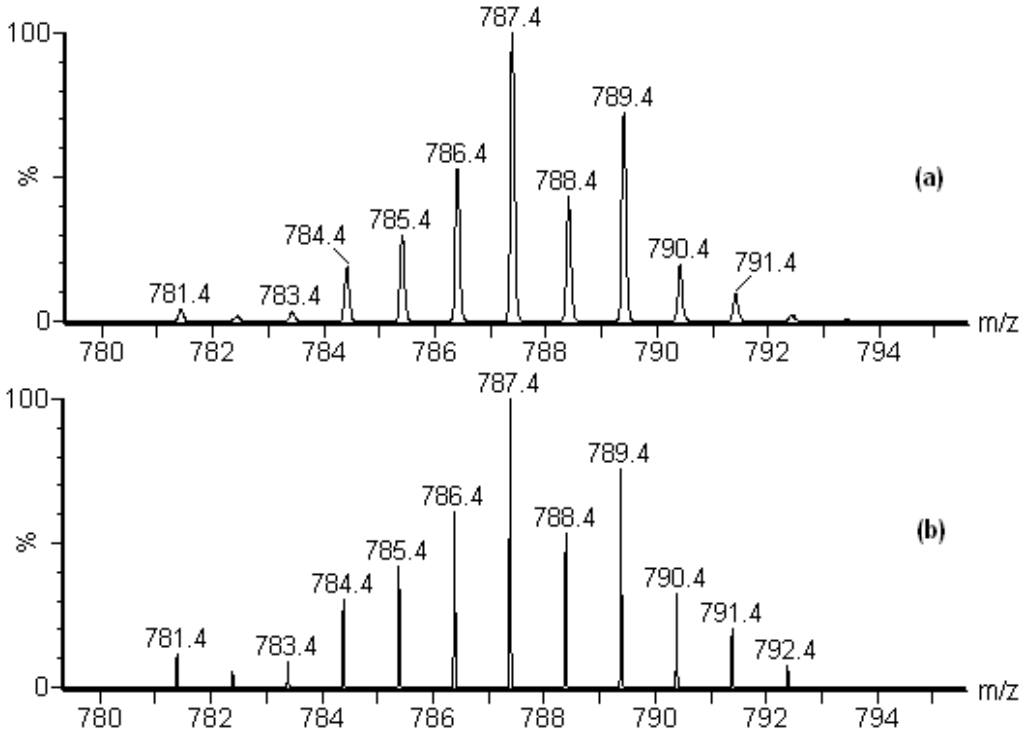

Figure S8. (a) Isotopic pattern of [**1**-Cl]$^+$; (b) theoretical isotopic pattern of [**1**-Cl]$^+$.

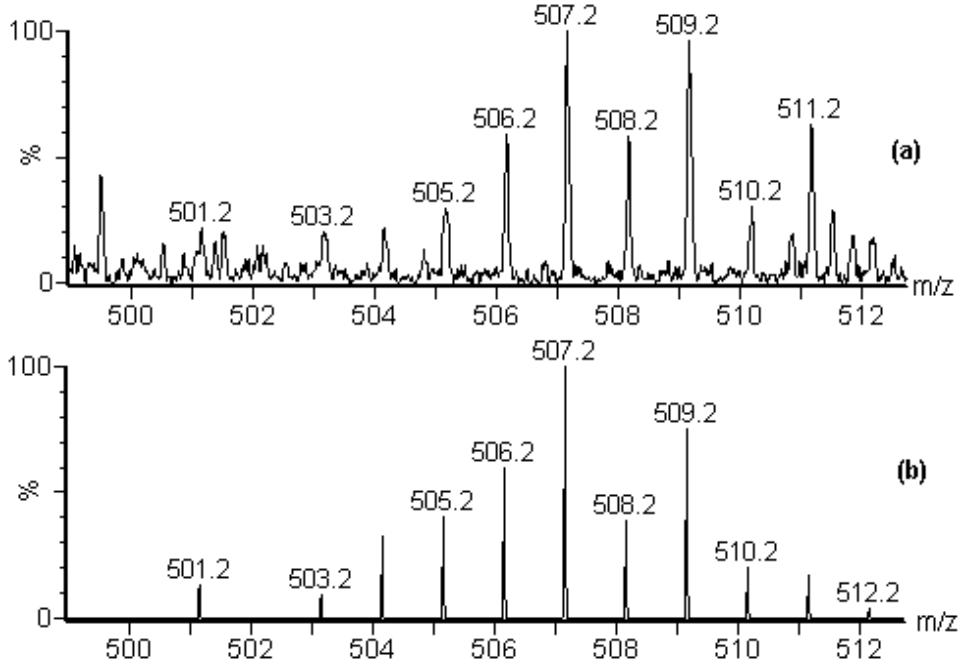

Figure S9. (a) Isotopic pattern of [**1a**-Cl]$^+$; (b) theoretical isotopic pattern of [**1a**-Cl]$^+$.

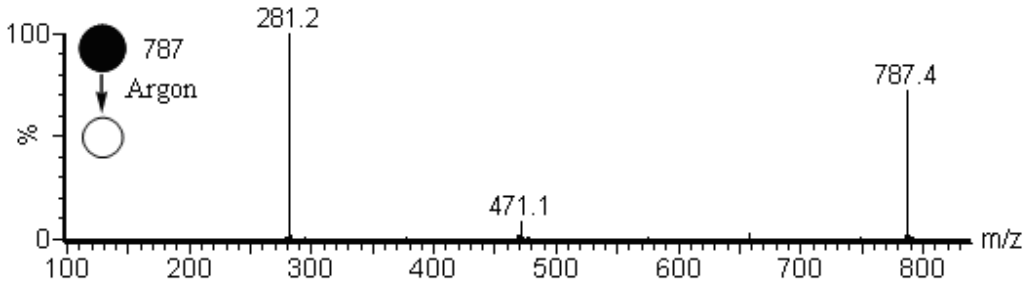

Figure S10. ESI MS/MS spectrum for CID of [**1**-Cl]$^+$ at *m/z* 787, the fragment ion at *m/z* 471 was generated by loss of phosphine PCy_3 (-280u) and HCl (-36u).

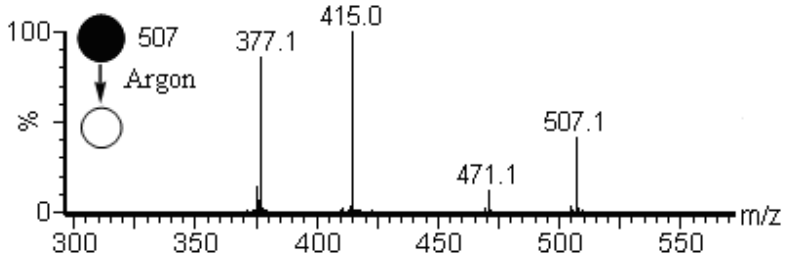

Figure S11. ESI MS/MS spectrum for CID of: (a) [**1a**-Cl]$^+$ at *m/z* 507, the fragment ion at 471 was generated by loss of HCl (-36u), the fragment ion at *m/z* 415 was generated by loss of toluene (-92u, carbene ligand (-90u) with H_2 (-2u)). Loss of toluene and HCl gives fragment ion at *m/z* 377. The gas phase mechanisms of loss of HCl and dehydrogenation of [**1a**-Cl]$^+$ at *m/z* 507 in MS/MS were proposed to be a C-H bond activation process through agostic interactions of coordinatively unsaturated Ru with the C-H bonds in the PCy_3 ligand (Scheme S1).

***Scheme S1*. Proposed Dissociation Pathways of [1a-Cl]$^+$**

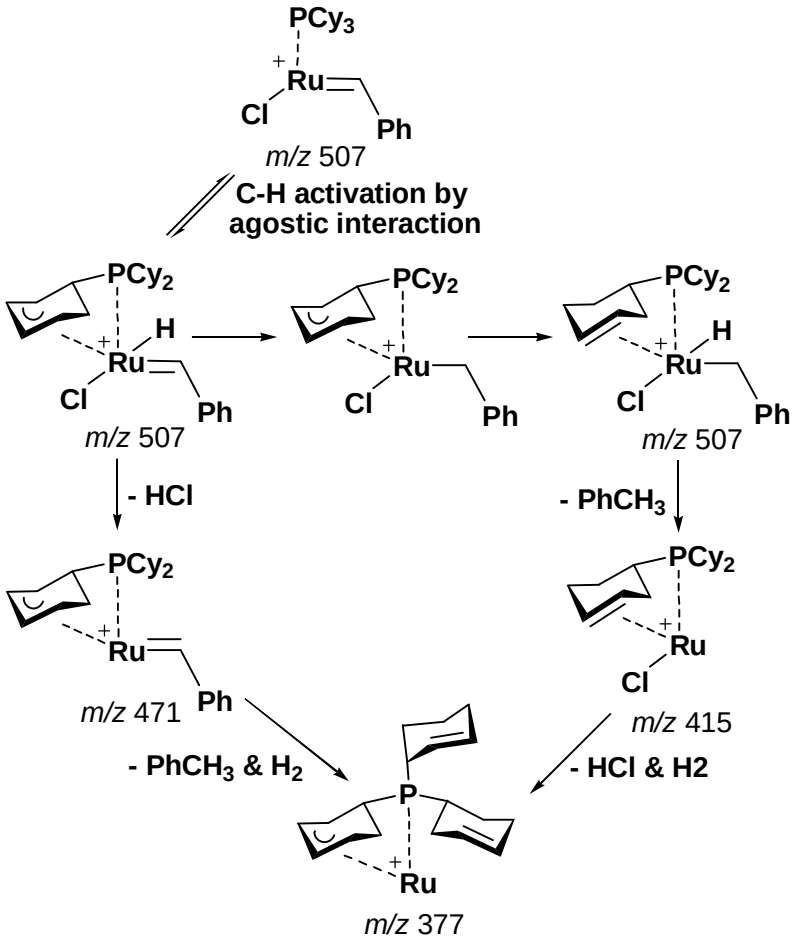

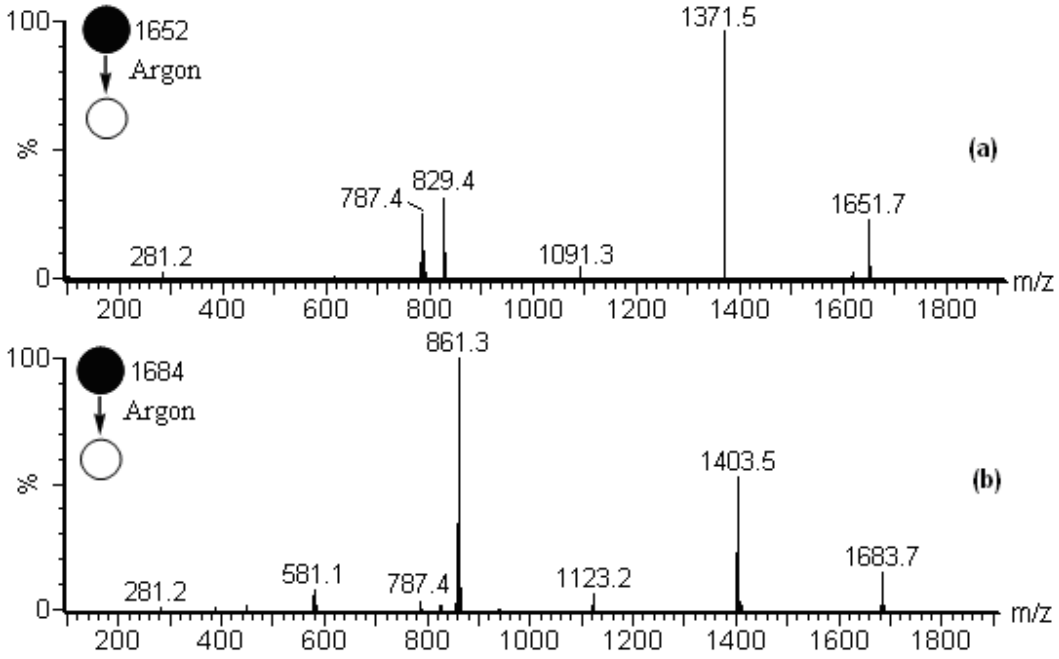

Figure S12. ESI-MS/MS spectra for CID of: (a) $\mathbf{1}_2 \cdot Li^+$ at *m/z* 1651.7; (a) $\mathbf{1}_2 \cdot K^+$ at *m/z* 1683.7

2. ESI MS spectra of alkali metal adduct ions of 2.

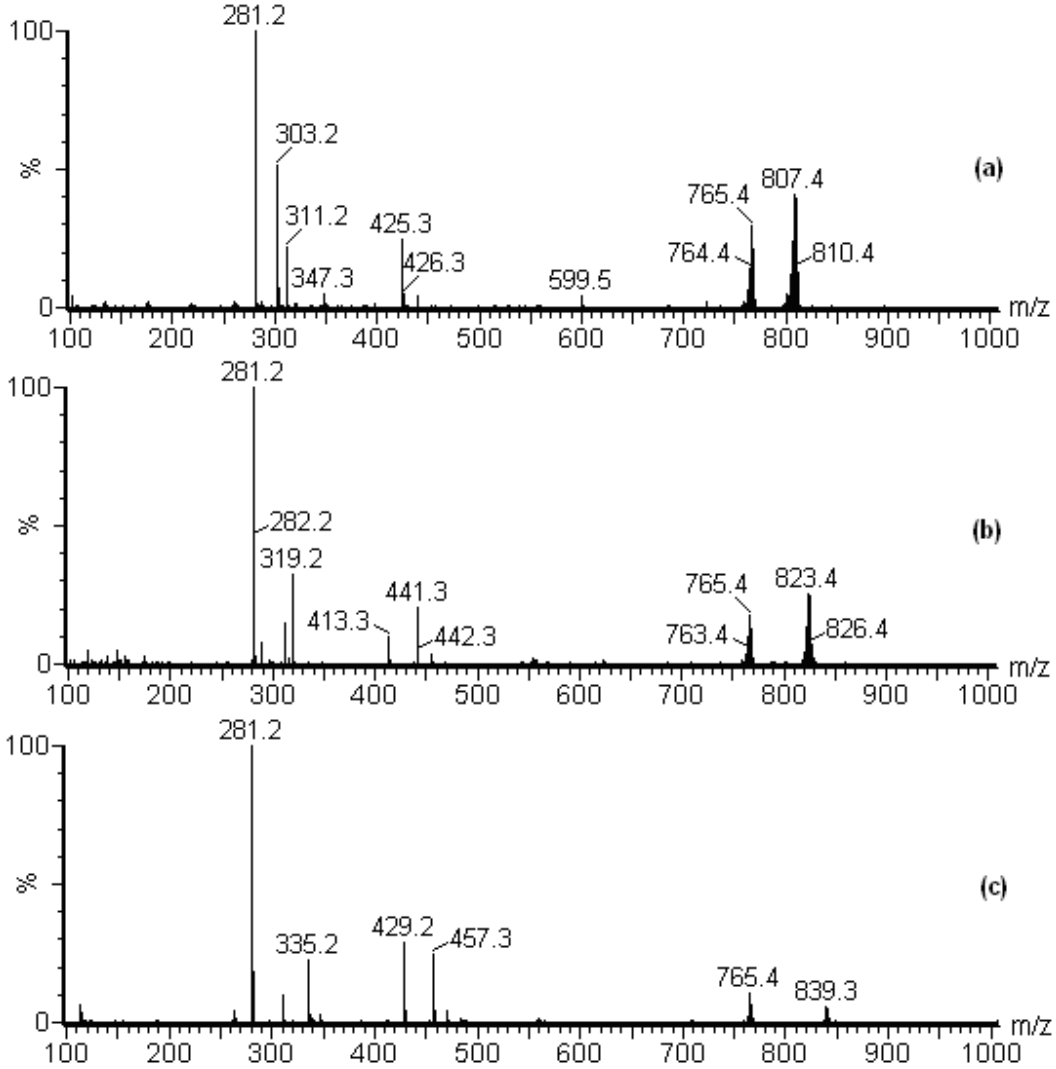

Figure S13. ESI mass spectra obtained by mixing the CH_3OH solution of alkali metal salt with the CH_2Cl_2 solution of **2** in an on-line micro-reactor, coupled the ESI ion source: (a) LiCl; (b) NaCl; (c) KCl.

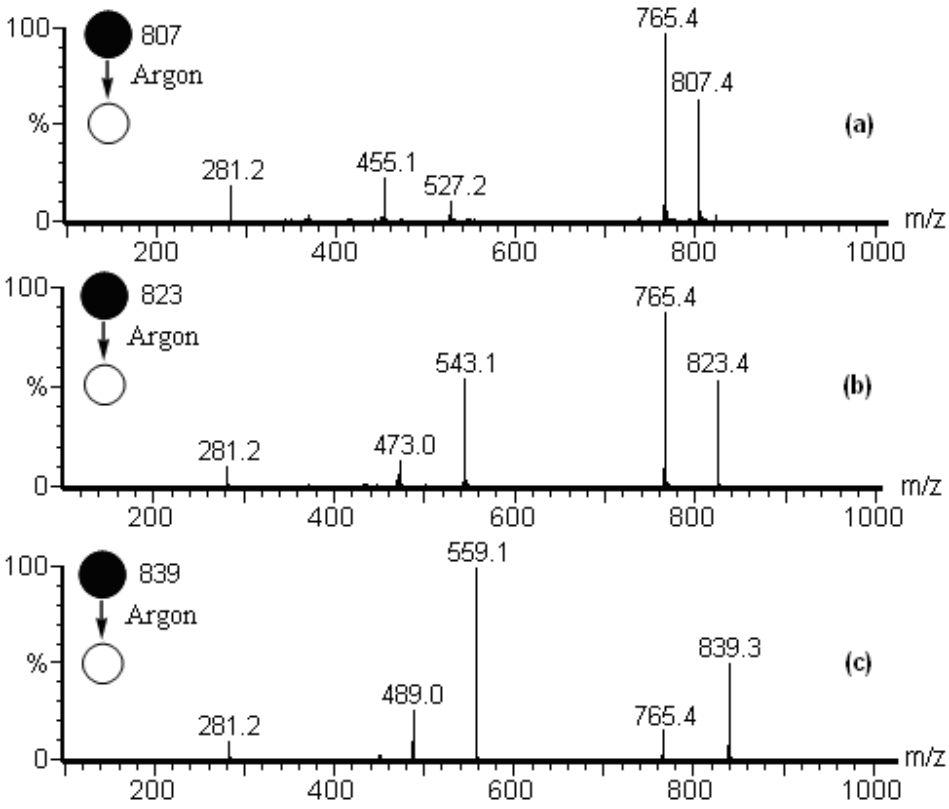

Figure S14. ESI-MS/MS spectra for CID of (a) **2**·Li^+ at *m/z* 807; (b) **2**·Na^+ at *m/z* 823; (c) **2**·K^+ at *m/z* 839

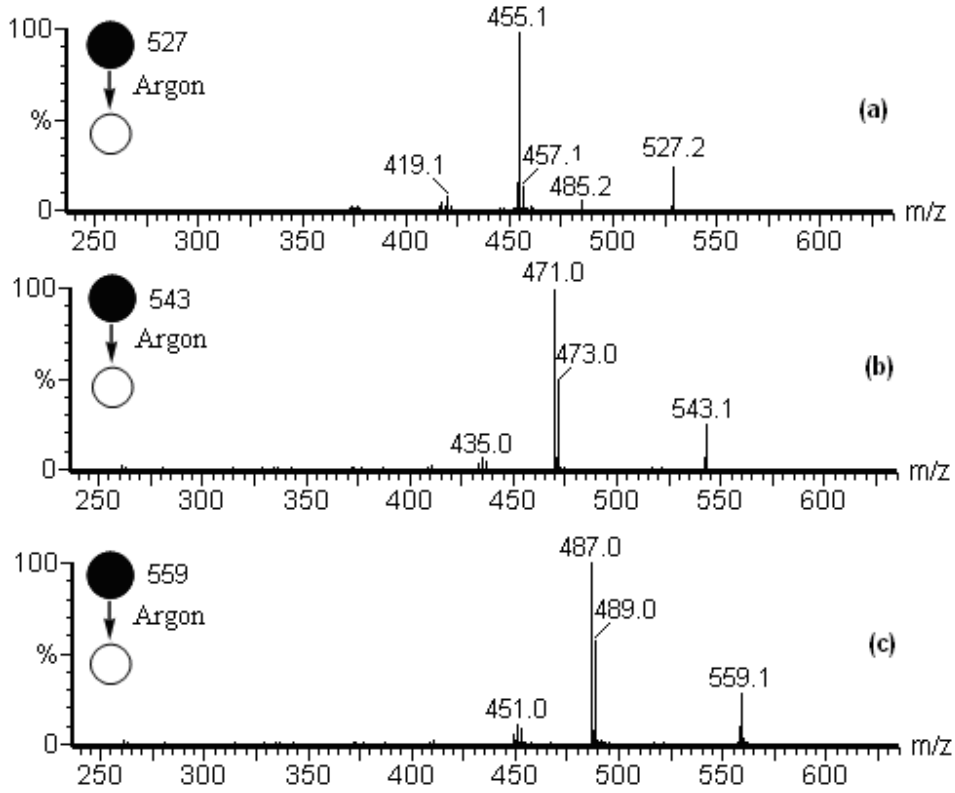

Figure S15. ESI-MS/MS spectra for CID of: (a) **2a**·Li^+ at *m/z* 527; (b) **2a**·Na^+ at *m/z* 543; (c) **2a**·K^+ at *m/z* 559

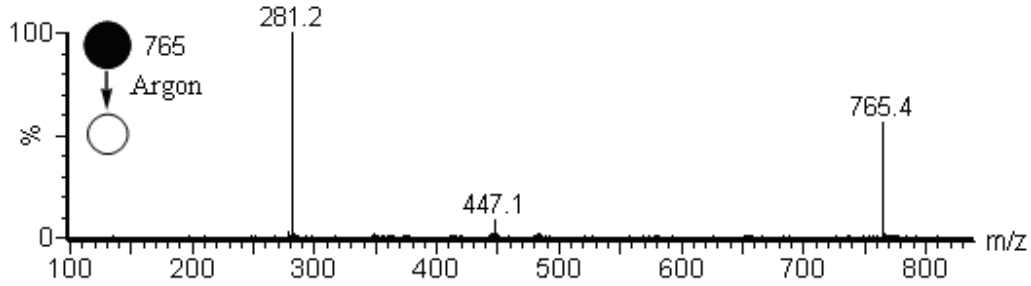

Figure S16. ESI MS/MS spectrum for CID of [**2**-Cl]$^+$ at *m/z* 765, the fragment ion at *m/z* 447 was generated by loss of phosphine PCy_3 (-280u) and HCl (-36u) with H_2 (-2u).

The ESI-MS/MS spectra for CID of **2**·M^+ (Figure S15) also showed two main fragments due to the loss of PCy_3 and of MCl, respectively, using a collision energy of 8~10eV. Interestingly, going from Li^+ over Na^+ to K^+ the intensity ratio of the fragment ions [[**2**-Cl]$^+$]/[**2a**·M^+] decreased in the same order of magnitude as in the respective

examples of **1**. Only 2eV collision energy could cause the dissociation of ions **2a**·M^+. Figures S15a-c showed the fragmentation ion series of **2a**·M^+ at *m/z*: (a) 457, 455 and 419; (b) 473, 471 and 435; (c) 489, 487 and 451 by loss of the 3-methylbut-2-enylidene ligand with H_2 (-70u) and $2H_2$ (-72u), respectively, and further loss of HCl (-36 u) with low intensity. The **2a**·Li^+ at *m/z* 527 shows the fragment ion at *m/z* 485 additionally by loss of LiCl.

The results of **2**·M^+ and **2a**·M^+ were similar to the respective results of **1**·M^+ and **1a**·M^+, which were discussed in details in the main paper. Thus the general fragmentation pathways for **1·M$^+$, 2·M$^+$, 1a·M$^+$** and **2a·M$^+$** were proposed and shown in Scheme S2 and the dissociation of **1a·M$^+$** and **2a·M$^+$** in MS/MS included the C-H bond activation process through agostic interactions of coordinatively unsaturated Ru with the C-H bonds in the PCy_3 ligand.

***Scheme S2*. Proposed Dissociation Pathways of 1·M$^+$, 2·M$^+$, 1a·M$^+$ and 2a·M$^+$**

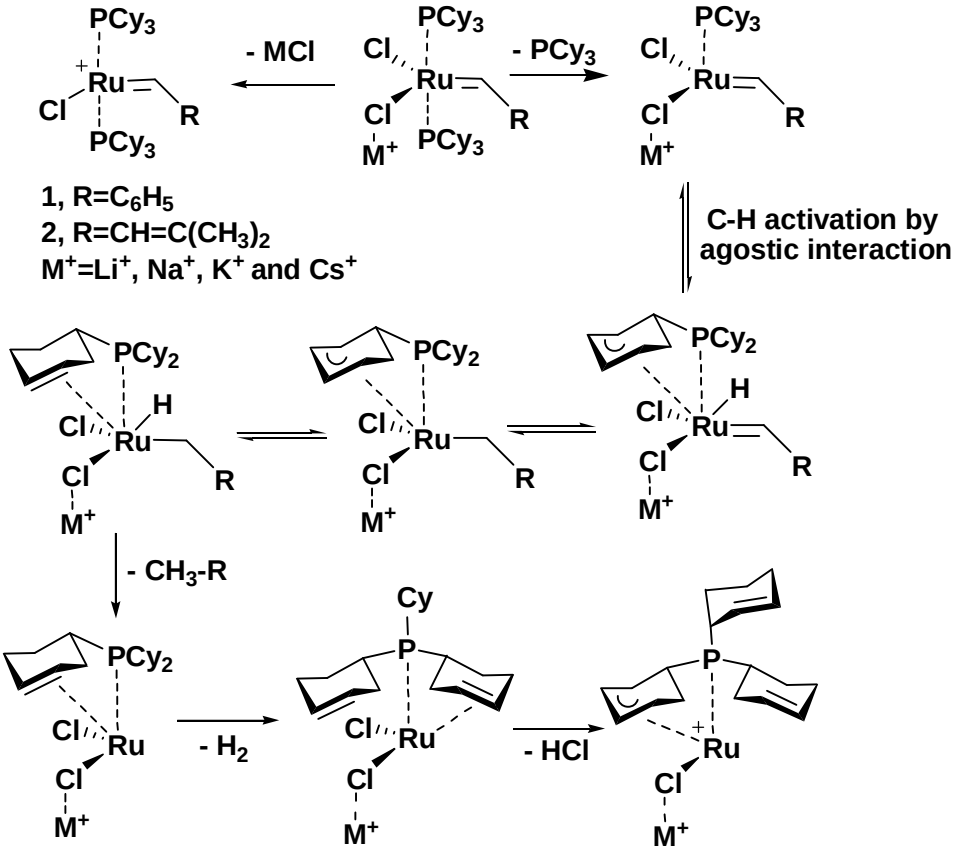

3. The influence of CH_3OH and LiCl onto the ESI mass spectrum of 1 in CH_2Cl_2

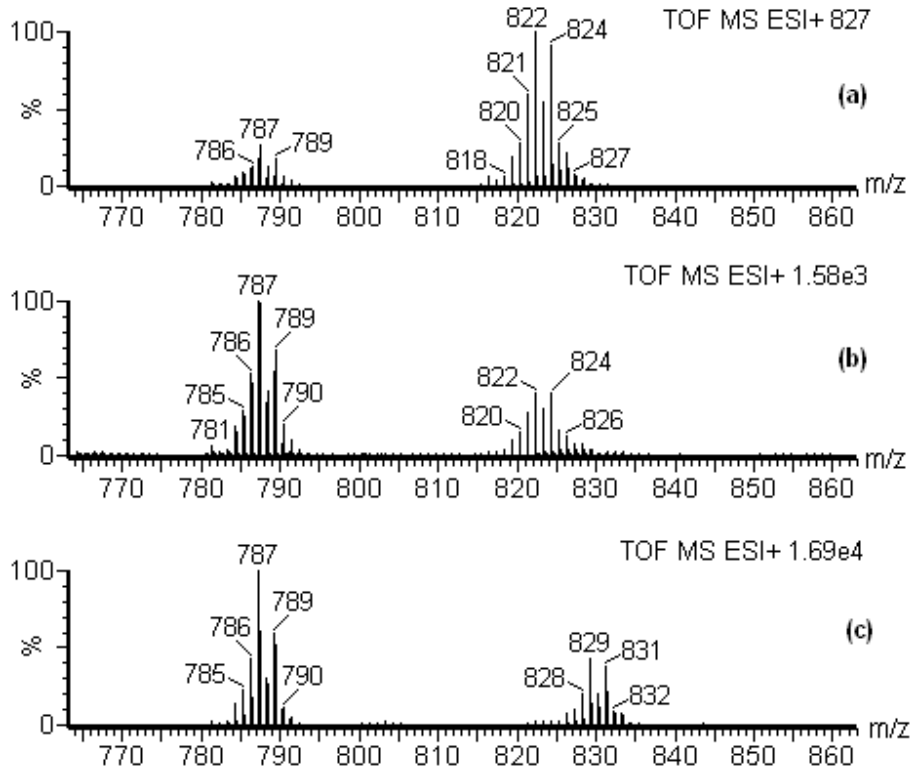

Figure S17. ESI mass spectra: (a) direct analysis of CH_2Cl_2 solution of **1** (5.5×10^{-5} M) with injection speed of 5μL/min; (b) addition of CH_3OH to the CH_2Cl_2 solution of **1** (5.5×10^{-5} M) using an injection speed of 5μL/min for both syringes in an on-line micro-reactor, coupled to the ESI source; (c) mixing the CH_3OH solution of LiCl (2.4×10^{-4} M) with the CH_2Cl_2 solution of **1** (5.5×10^{-5} M) using an injection speed of 5μL/min for both syringes.

The results presented in Figure S17 give evidence that using alkali metal cationization the detection sensitivity will be enhanced approximately 10 times in comparison to direct analysis.

4. Ion-molecule reactions of Li^+ or K^+ adduct ions of Ru-catalyst 1 with 1-butene or ethene

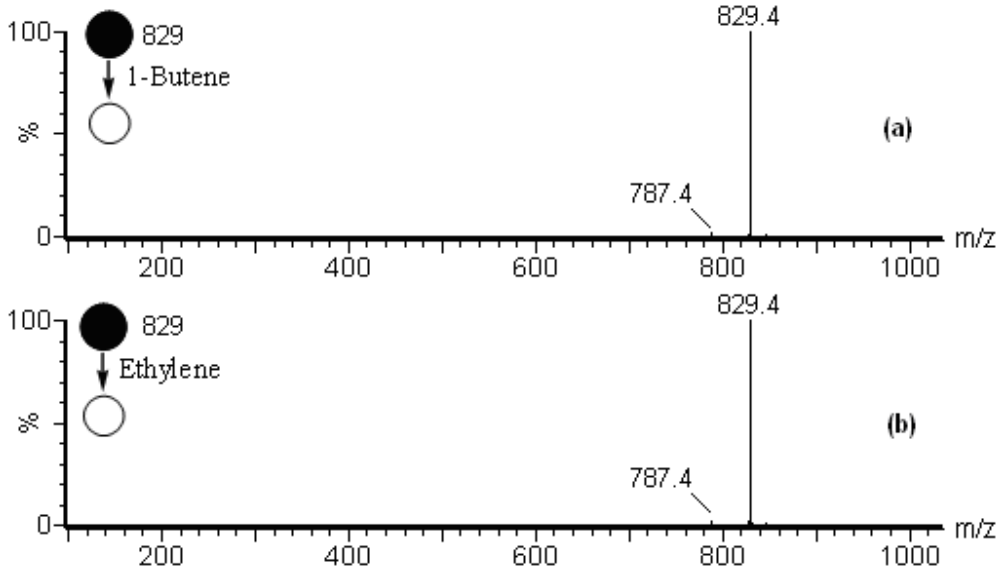

Figure S18. Mass spectra of ion-molecule reaction of **1**·Li^+ at *m/z* 829 with: (a) 1-butene; (b) ethene. No metathesis product was detected.

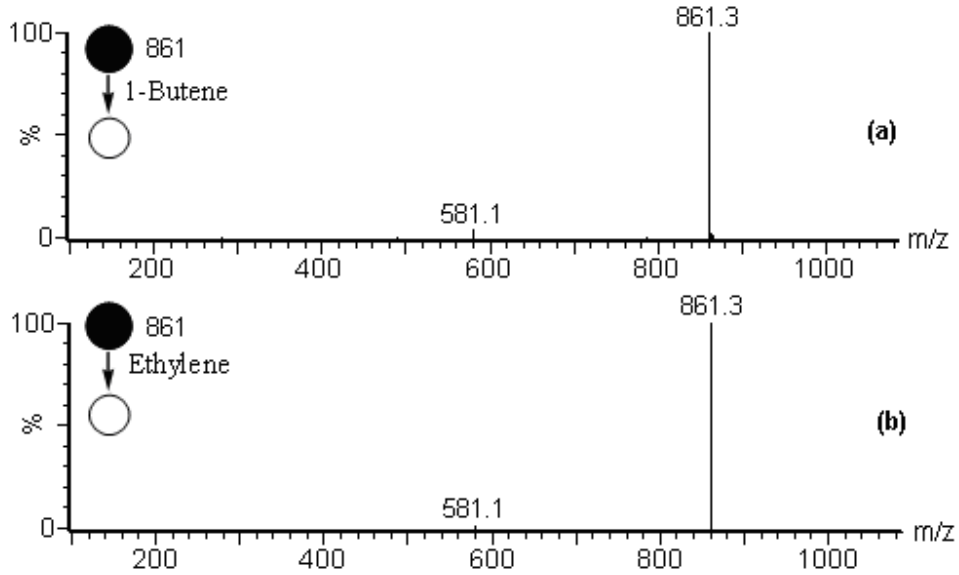

Figure S19. Mass spectra of ion-molecule reaction of **1**·K^+ at *m/z* 861 with: (a) 1-butene; (b) ethene. No metathesis product was detected.

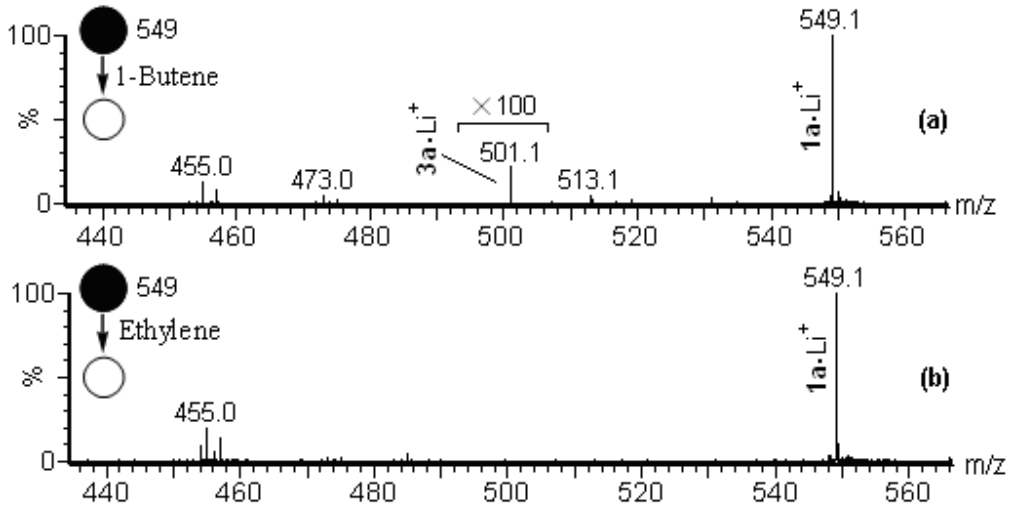

Figure S20. Mass spectra of ion-molecule reaction of **1a**·Li^+ at *m/z* 549 with: (a) 1-butene; (b) ethene. The metathesis product **3a**·Li^+ at *m/z* 501 (the intensity of **3a**·Li^+ at *m/z* 501 was enhanced ×100) was detected, however, no metathesis product was observed in the reaction of **1a**·Li^+ with ethene.

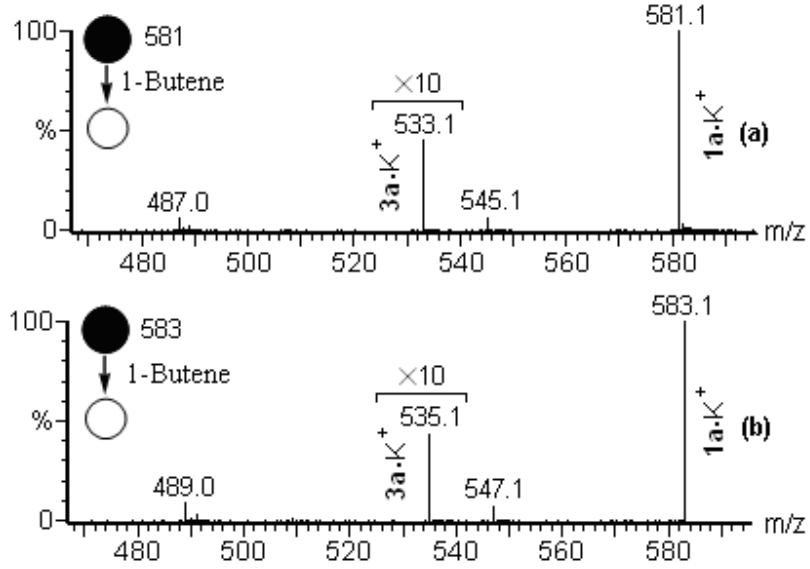

Figure S21. Mass spectra of ion-molecule reaction of **1a**·K^+ at (a) *m/z* 581; (b) *m/z* 583, with 1-butene. The metathesis product **3a**·K^+ at (a) *m/z* 533 (the intensity of **3a**·K^+ at *m/z* 533 was enhanced ×10); (b) *m/z* 535 (the intensity of **3a**·K^+ at *m/z* 535 was enhanced ×10), were observed. The ion at (a) *m/z* 545; (b) *m/z* 547, were products of the

ion-molecule reaction of fragment ions at (a) *m/z* 489; (b) *m/z* 491, with 1-butene.

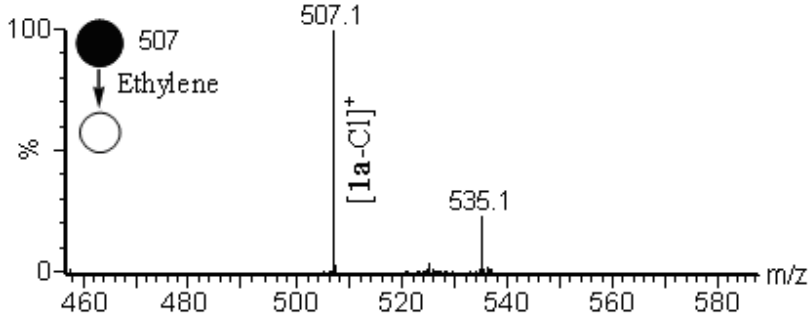

Figure S22. Mass spectrum of ion-molecule reaction of [**1a**-Cl]$^+$ at *m/z* 507 with ethene. The adduct ion at *m/z* 535 was detected.

5. RCM reactions of a,? -dienes (5-7) with catalyst 1 in presence of KCl

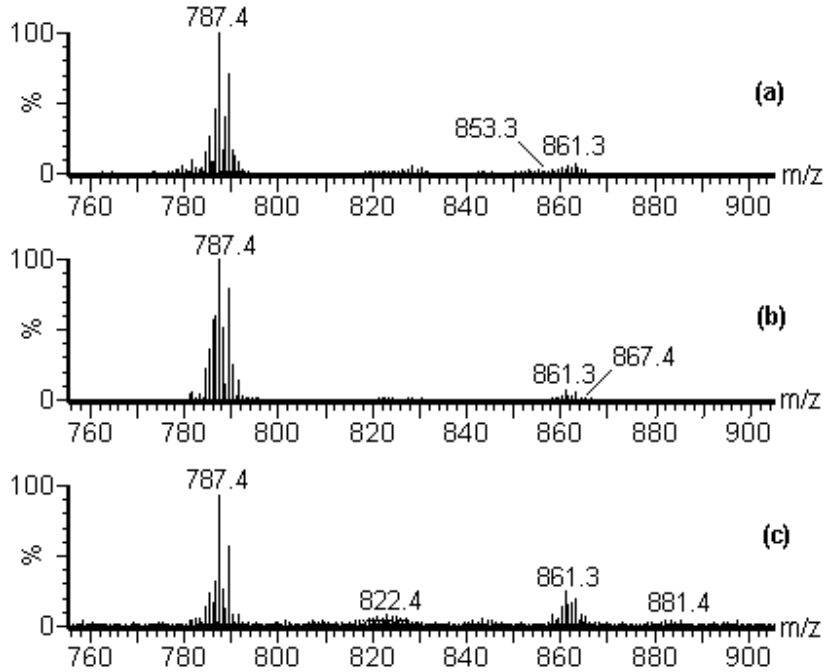

Figure S23. ESI mass spectra of RCM reactions of dienes: (a) 1,6-Heptadiene **5**; (b) 1,7-Octadiene **6**; (c) 1,8-Nonadiene **7**, with catalyst **1** in presence of KCl. The reaction time was approximately 12 s. The K^+ adduct ions of alkylidene Ru intermediates were observed as (a) **8**·K^+ at *m/z* 853, (b) **9**·K^+ at *m/z* 867, (c) **10**·K^+ at *m/z* 881. The signals of

1·K^+ at *m/z* 861 and of [**1**-Cl]$^+$ at *m/z* 787 are still present.

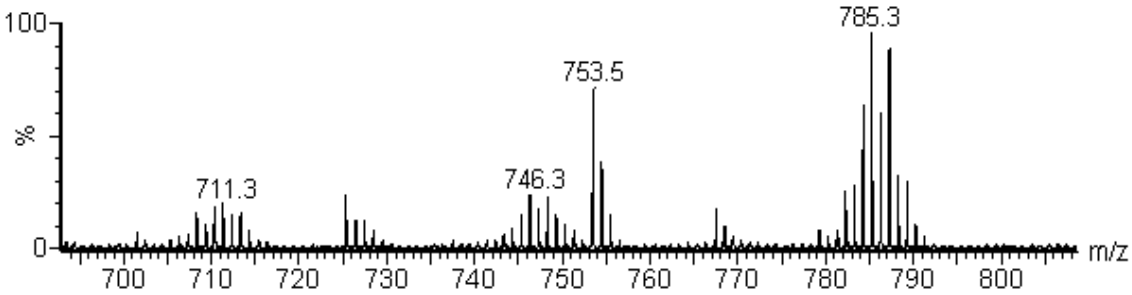

Figure S24. ESI mass spectrum the RCM reaction after 1 hour reaction time showing **4**·K^+ at *m/z* 785 and **4**$^{\bullet+}$ at *m/z* 746. The reaction solution of catalyst **1** and 1,7-Octadiene **6** in CH_2Cl_2 was mixed after 1 hour with a CH_3OH solution of KCl in the micro-reactor coupled to ESI-MS,.

The signals of some intermediates of low intensity, such as **8a**·K^+ at *m/z* 573 and **9a**·K^+ at *m/z* 587,could be characterized by MS/MS. After 1 hour reaction time the respective signals of the benzylidene **1**·K^+ at *m/z* 861 and alkylidene Ru complexes **8**·K^+ at *m/z* 853 disappeared and the mass spectrum showed **4**·K^+ at *m/z* 785 (isotopic pattern shown in Figure S25), 4$^{\bullet+}$ at *m/z* 746, [**4**-Cl]$^+$ at *m/z* 711, and even **4a**·K^+ at *m/z* 505 (isotopic pattern shown in Figure S26).

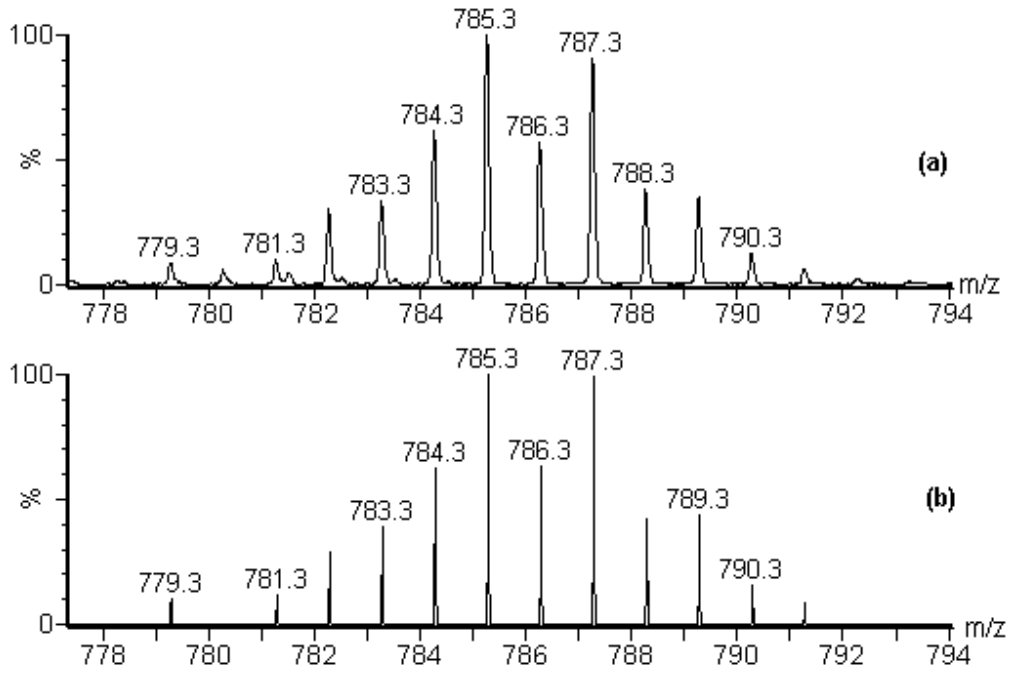

Figure S25. (a) Isotopic pattern of **4**·K^+; (b) theoretical isotopic pattern of **4**·K^+.

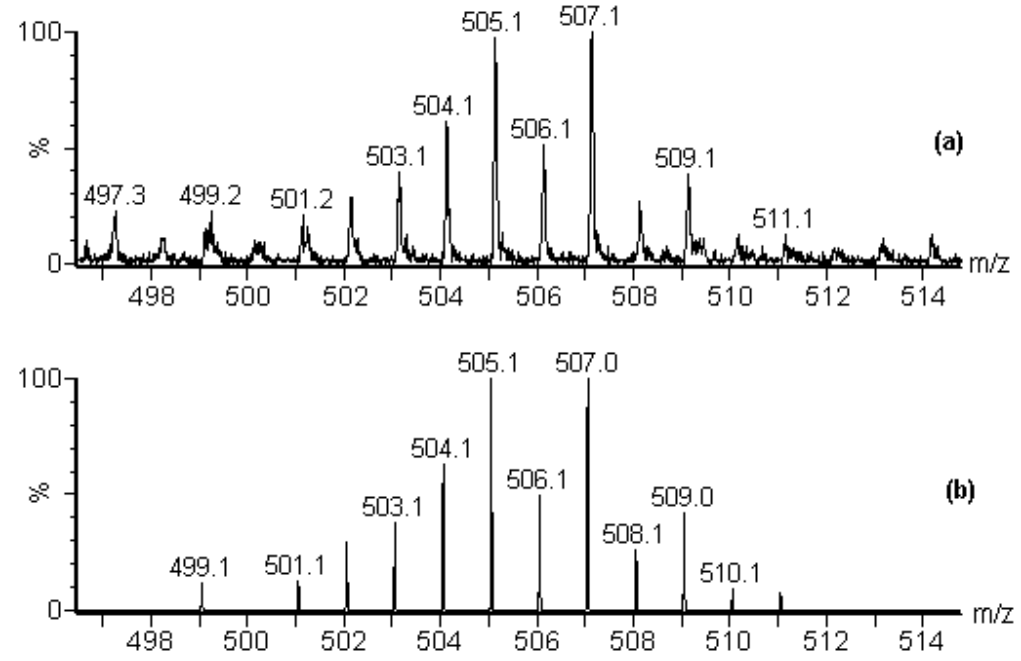

Figure S26. (a) Isotopic pattern of **4a**·K^+; (b) theoretical isotopic pattern of **4a**·K^+.

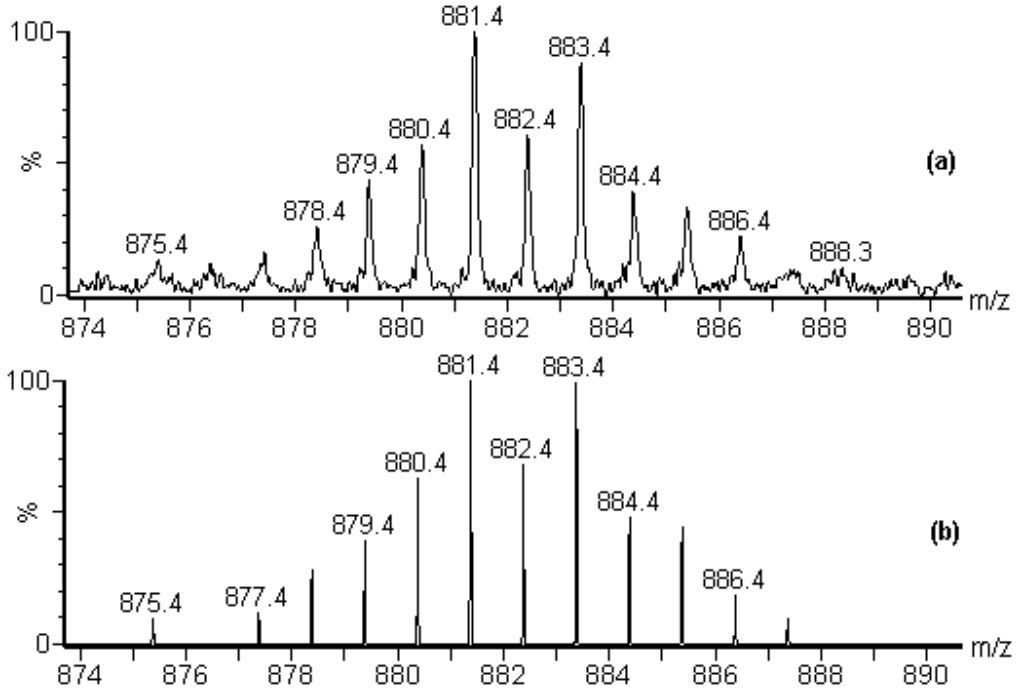

Figure S27. (a) Isotopic pattern of **10**·K^+; (b) theoretical isotopic pattern of **10**·K^+.

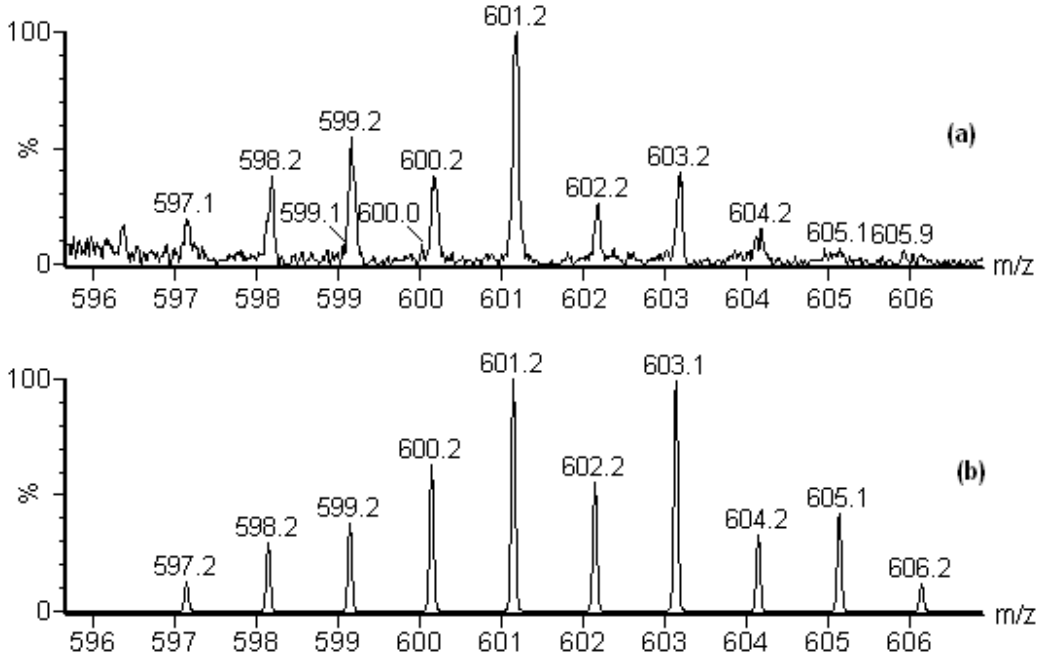

Figure S28. (a) Isotopic pattern of **10a**·K^+; (b) theoretical isotopic pattern of **10a**·K^+.

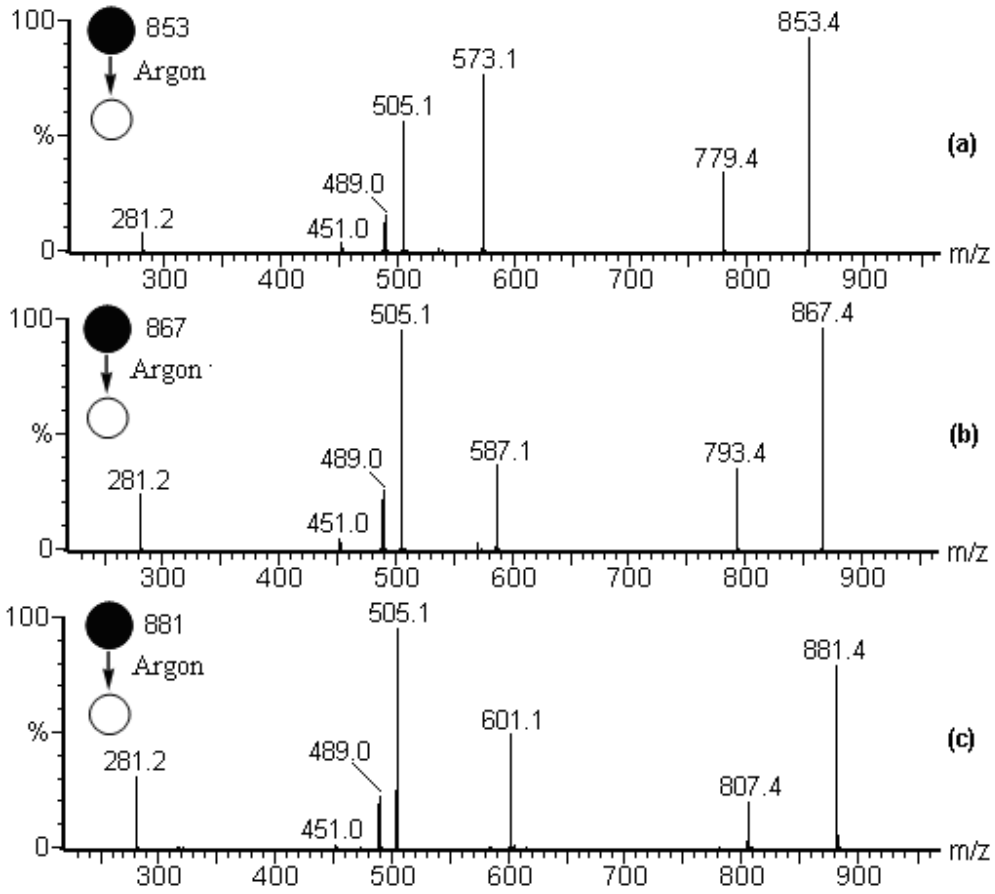

Figure S29. ESI MS/MS spectra for CID of: (a) **8**·K^+ at *m/z* 853; (b) **9**·K^+ at *m/z* 867; (c) **10**·K^+ at *m/z* 881.

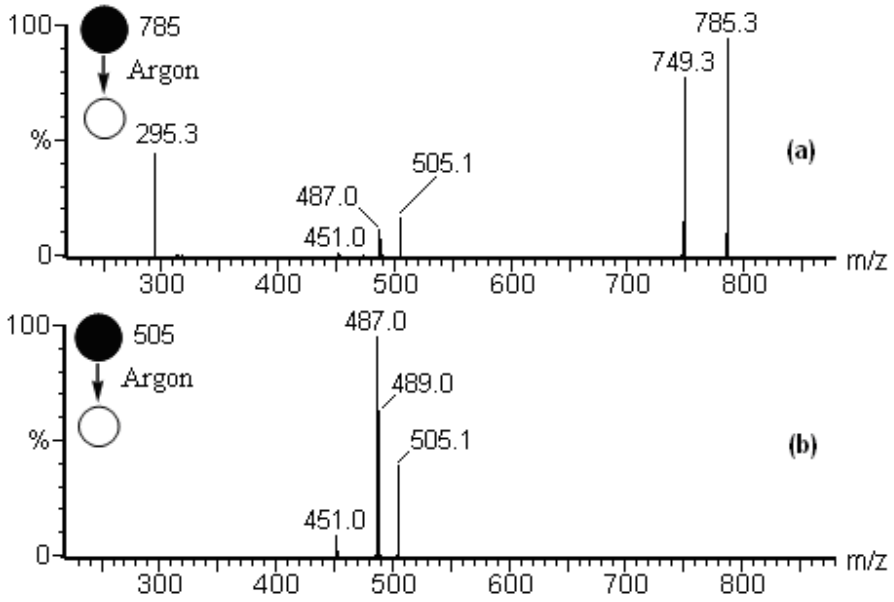

Figure S30. ESI-MS/MS spectra for CID of: (a) **4**·K^+ at *m/z* 785; (b) **4a**·K^+ at *m/z* 505.

6. ADMET polymerization reaction of 1,9-decadiene (14) with catalyst 1 in presence of KCl

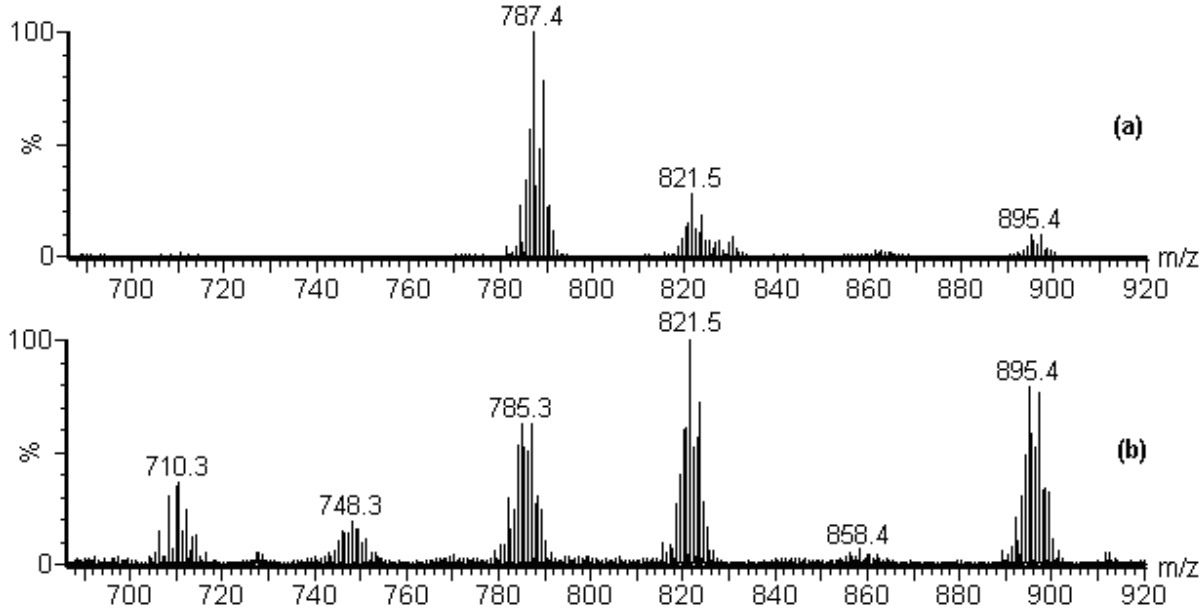

Figure S31. ESI mass spectra of ADMET polymerization reaction (a) by mixing a CH_2Cl_2 solution of **1** with a CH_3OH solution of 1,9-decadiene **14** in presence of KCl, the reaction time was 12s. The signal of **15**·K^+ at *m/z* 895 was detected with low intensity.

(b) first adding 1,9-decadiene **14** to the CH_2Cl_2 solution of **1**, then after 1 hour of reaction time mixing the reaction solution with a CH_3OH solution of KCl. The signal of **15**·K^+ at *m/z* 895 was increased significantly. The signals of the **1**·K^+ and [**1**-Cl]$^+$ at *m/z* 787 disappeared and the mass spectrum showed **4**·K^+ at *m/z* 785.

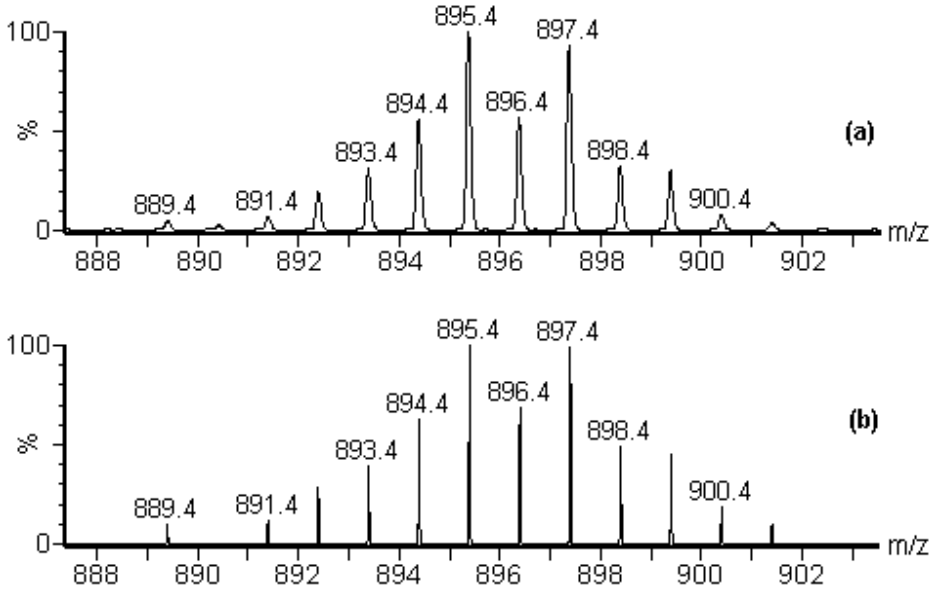

Figure S32. (a) Isotopic pattern of **15**·K^+; (b) theoretical isotopic pattern of **15**·K^+.

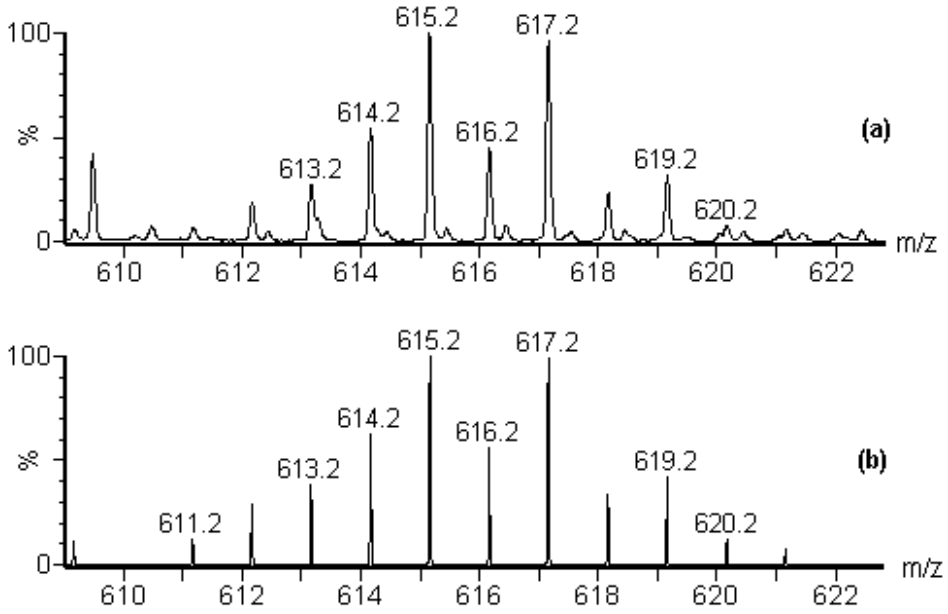

Figure S33. (a) Isotopic pattern of **15a**·K^+; (b) theoretical isotopic pattern of **15a**·K^+.

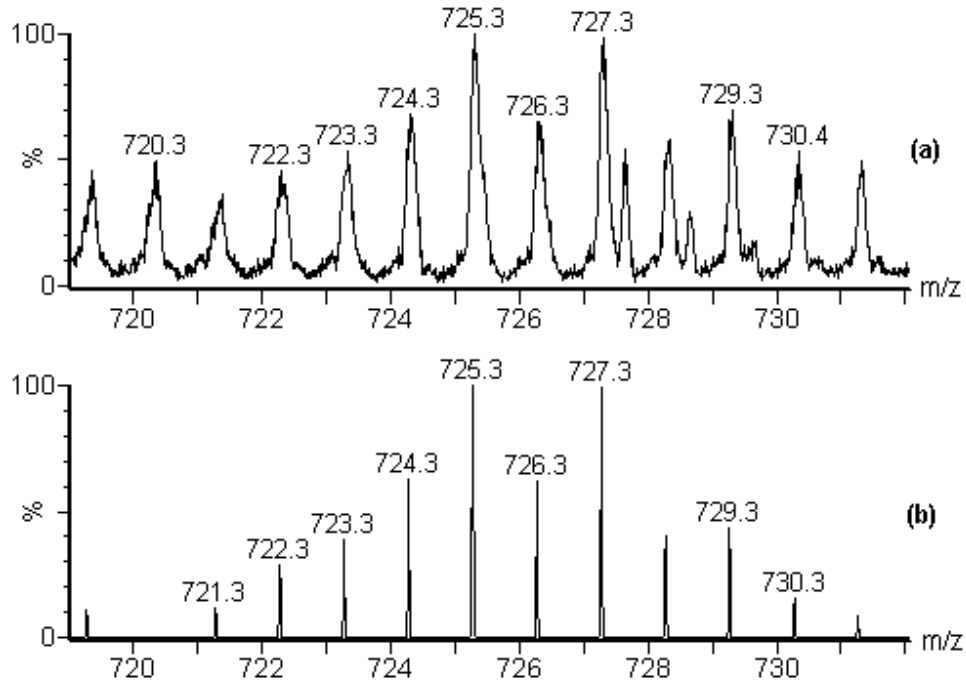

Figure S34. (a) Isotopic pattern of **16a**·K^+; (b) theoretical isotopic pattern of **16a**·K^+.

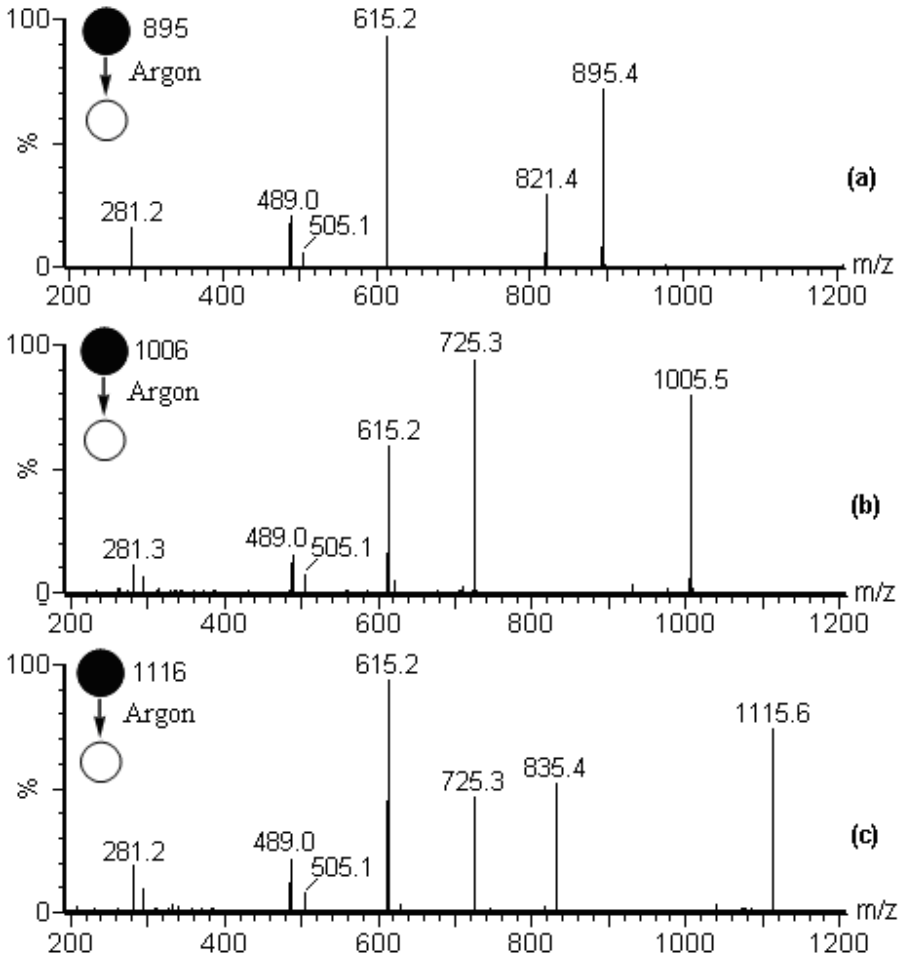

Figure S35. ESI MS/MS spectra of: (a) **15**·K^+ at *m/z* 895.4; (b) **16**·K^+ at *m/z* 1005.5; (c) **17**·K^+ at *m/z* 1115.6.

7. ROMP reaction of cyclooctene 18 with catalyst 1 in presence of KCl

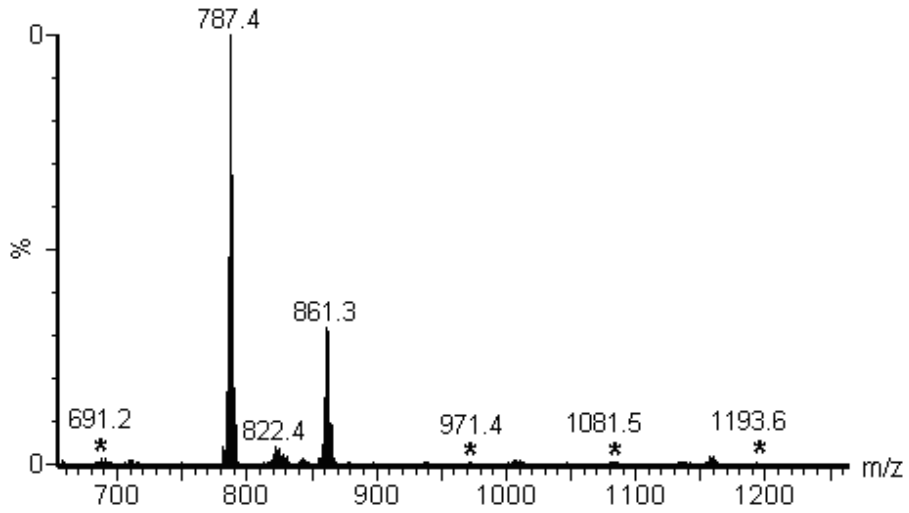

Figure S36. ESI mass spectrum of the ROMP reaction by mixing a CH_2Cl_2 solution of **1** with a CH_3OH solution of cyclooctene **18** in presence of KCl, the reaction time was 12s. **19a**·K^+ at *m/z* 691, **19**·K^+ at *m/z* 971, **20**·K^+ at *m/z* 1081 and **21**·K^+ at *m/z* 1191 (marked with "*"). The intensities of **19a**·K^+ at *m/z* 691, **19**·K^+ at *m/z* 971, **20a**·K^+ at *m/z* 801, **20**·K^+ at *m/z* 1081 and **21a**·K^+ at *m/z* 911, **21**·K^+ at *m/z* 1191, were 148, 70, 47, 125, 28 and 65, respectively. The signals of **1**·K^+ at *m/z* 861 and of [**1**-Cl]$^+$ at *m/z* 787 are still present with high intensity.

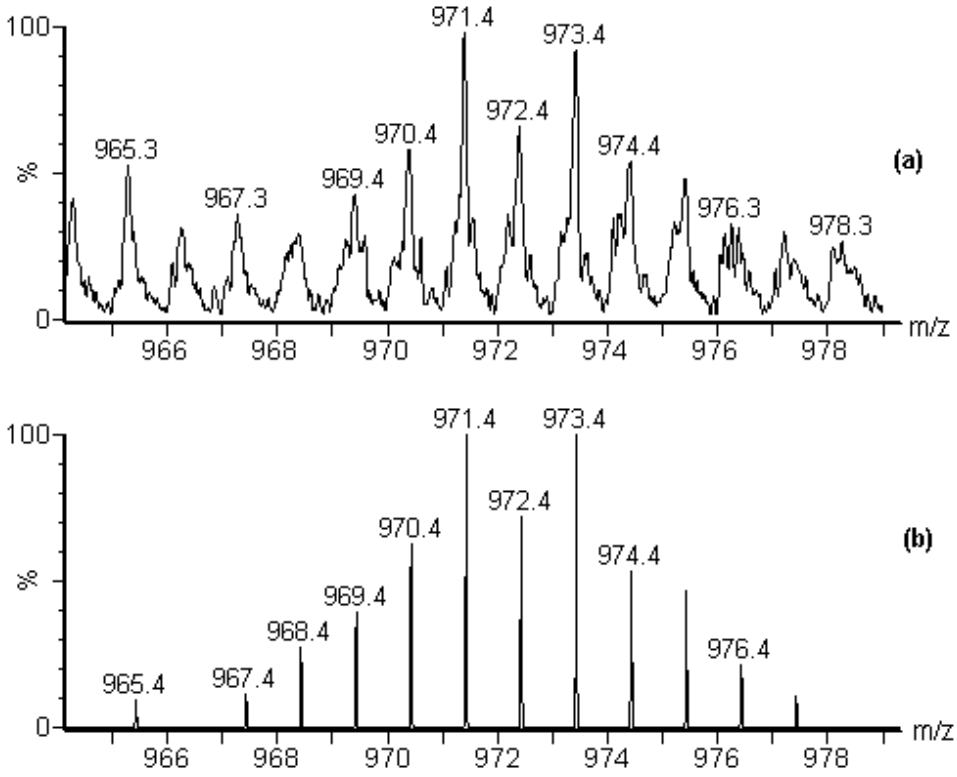

Figure S37. (a) Isotopic pattern of **19**·K^+; (b) theoretical isotopic pattern of **19**·K^+.

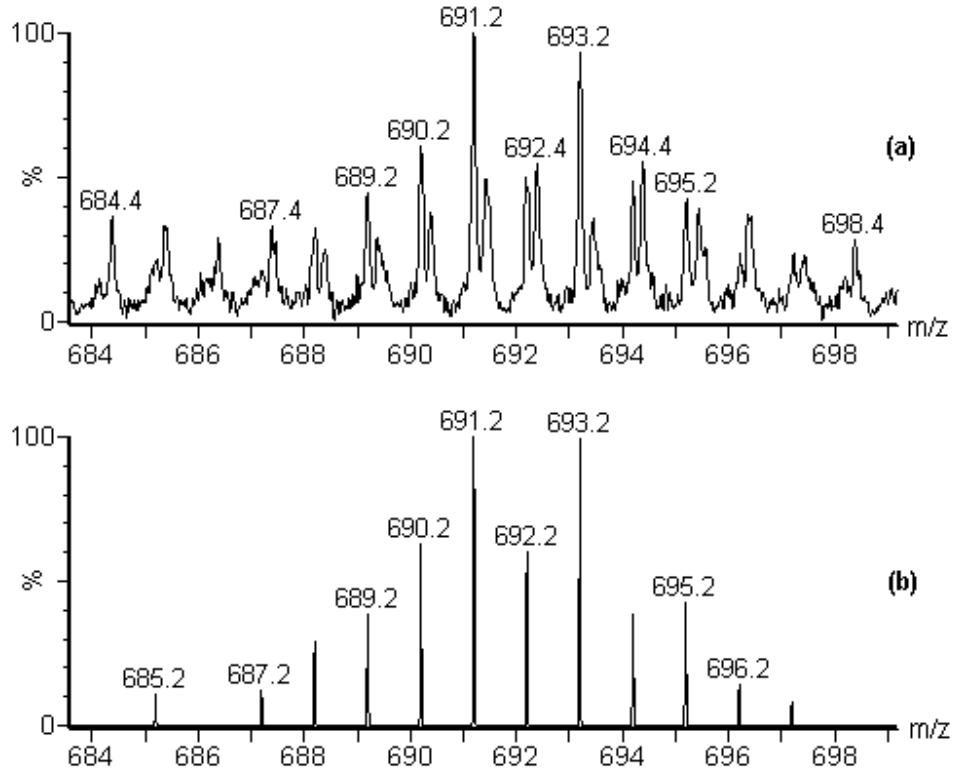

Figure S38. (a) Isotopic pattern of **19a**·K^+; (b) theoretical isotopic pattern of **19a**·K^+.

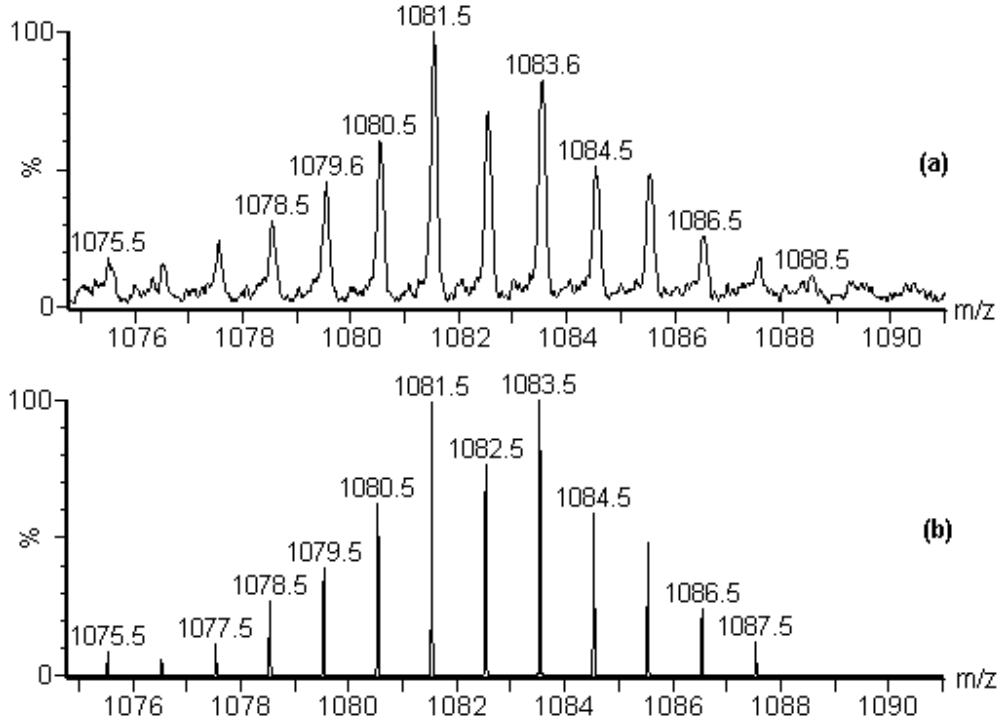

Figure S39. (a) Isotopic pattern of **20**·K^+; (b) theoretical isotopic pattern of **20**·K^+.

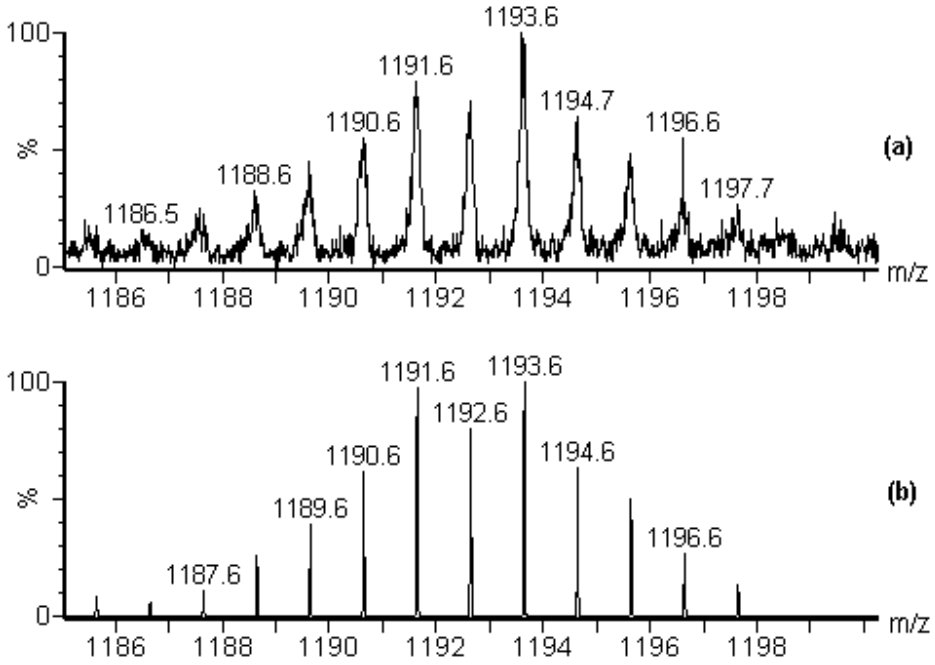

Figure 40. (a) Isotopic pattern of **21**·K^+; (b) theoretical isotopic pattern of **21**·K^+.

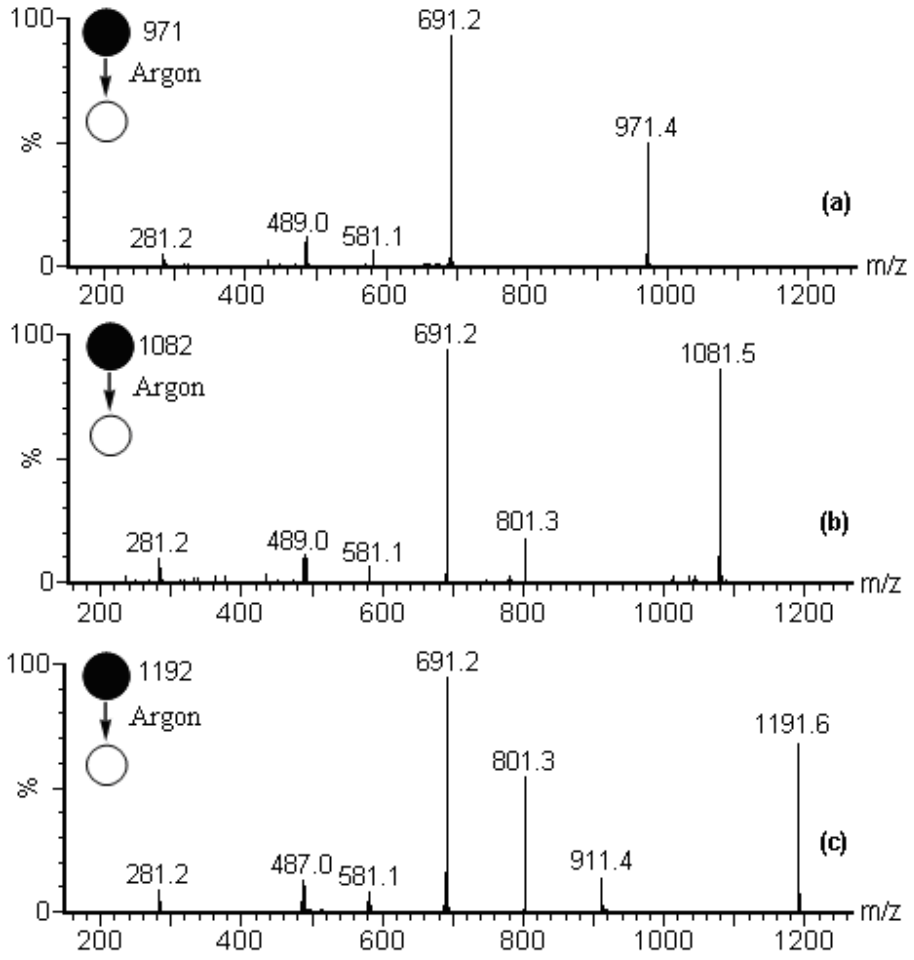

Figure S41. ESI MS/MS spectra of: (a) **19**·K^+ at *m/z* 971.4; (b) **20**·K^+ at *m/z* 1081.5; (c) **21**·K^+ at *m/z* 1191.6.

8. Reaction of 1,5-hexadiene 22 with catalyst 1.

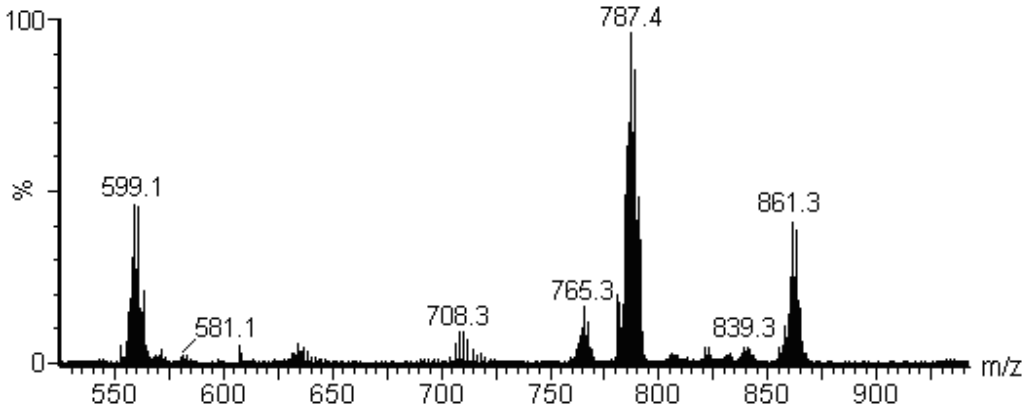

Figure S42. ESI mass spectrum the reaction of catalyst **1**, dissolved in CH_2Cl_2, with of 1,5-hexadiene in presence of KCl, dissolved in methanol. The reaction time was 12s. The intensity of the monophosphine Ru-species **23a**·K^+ at *m/z* 559 was observed "abnormally" much higher than of the bisphosphine Ru-species **23**·K^+ at *m/z* 839, which provided clear evidence for intramolecular p-complexation within **23a**.

9. Computational results

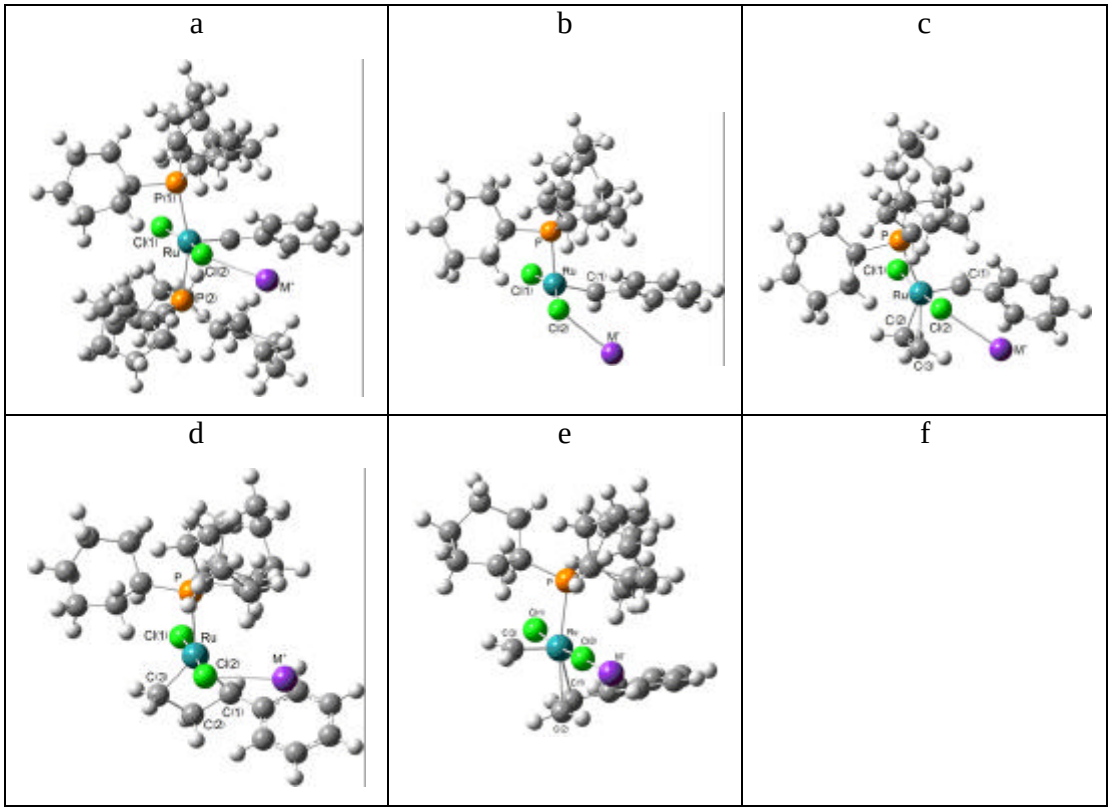

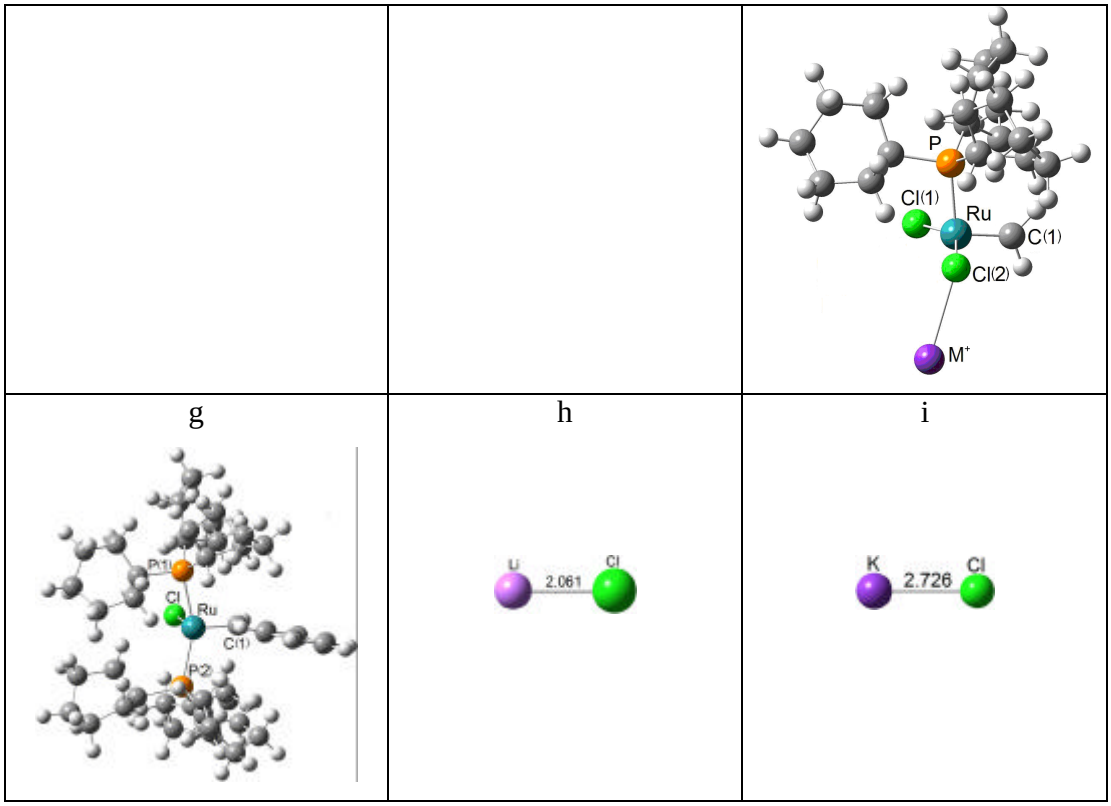

Figure S43. Ball and stick models of a) **1**·M^+; b) **1a**·M^+; c) first p-complex [**1a**·M^+ + ethene]; d) Ru-cyclobutane intermediate $(PCy_3)(C_9H_{10})RuCl_2 \cdot M^+$; e) second p-complex [**4a**·M^+ + styrene]; f) **4a**·M^+; g) [**1**-Cl]$^+$; h) LiCl; i) KCl. (M^+= Li^+ or K^+). Table S1-S7 give detailed information about the corresponding structures.

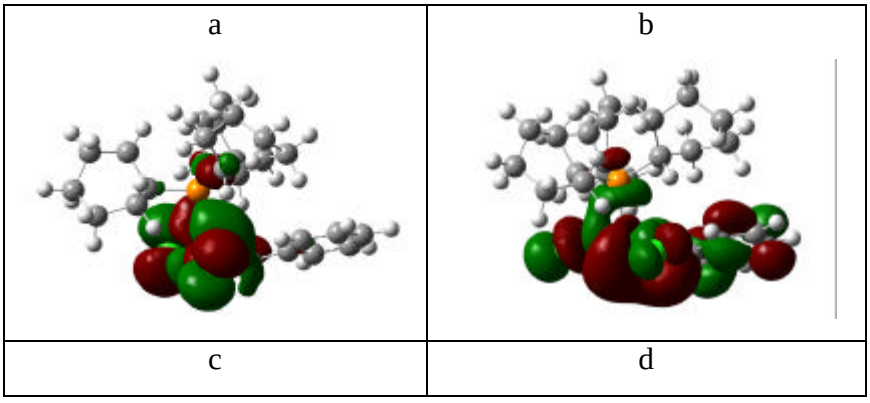

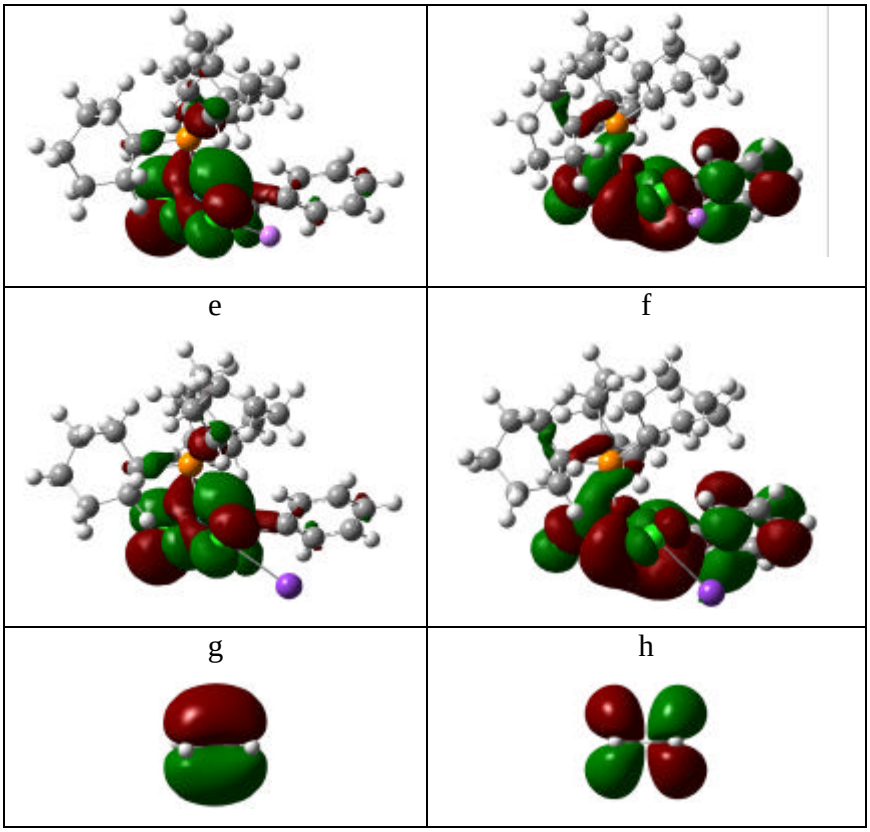

Figure S44. Molecular orbital diagrams of (a) **1a** (HOMO); (b) **1a** (LUMO); (c) **1**·Li^+ (HOMO); (d)**1**·Li^+ (LUMO); (e) **1a**·K^+ (HOMO); (f) **1a**·K^+ (LUMO); (g) C_2H_4 (HOMO); (h) C_2H_4 (LUMO).

Table S1. Structural parameters of **1**, **1**·Li^+ and **1**·K^+.

Structural parameters	**1**	**1**·Li^+	**1**·K^+
Ru-$Cl_{(1)}$ (Å)	2.458	2.404	2.409
Ru-$Cl_{(2)}$ (Å)	2.458	2.521	2.519
Ru-$P_{(1)}$ (Å)	2.447	2.500	2.501
Ru-$P_{(2)}$ (Å)	2.474	2.522	2.484
Ru-$C_{(1)}$ (Å)	1.855	1.870	1.852
$Cl_{(1)}$-Ru-$Cl_{(2)}$ (degree)	161.1	165.4	163.9
$P_{(1)}$-Ru-$P_{(2)}$ (degree)	164.2	160.5	161.2
M^+-$Cl_{(2)}$ (Å)	--	2.185	2.959

$Ru\text{-}Cl_{(2)}\text{-}M^+$ (degree)	--	68.8	120.7
$P_{(1)}\text{-}Ru\text{-}Cl_{(2)}\text{-}M^+$ (degree)	--	-134.6	-121.5

Table S2. Structural parameters of **1a**, **1a**·Li^+ and **1a**·K^+.

Structural parameters	**1a**	**1a**·Li^+	**1a**·K^+
$Ru\text{-}Cl_{(1)}$ (Å)	2.374	2.330	2.341
$Ru\text{-}Cl_{(2)}$ (Å)	2.365	2.459	2.428
Ru-P (Å)	2.279	2.307	2.302
$Ru\text{-}C_{(1)}$ (Å)	1.835	1.865	1.851
$Cl_{(1)}\text{-}Ru\text{-}Cl_{(2)}$ (degree)	151.3	157.1	155.1
$M^+\text{-}Cl_{(2)}$ (Å)	--	2.211	2.977
$Ru\text{-}Cl_{(2)}\text{-}M^+$ (degree)	--	80.3	96.3
$P_{(1)}\text{-}Ru\text{-}Cl_{(2)}\text{-}M^+$ (degree)	--	-120.9	-134.6

Table S3. Structural parameters of [**1**-Cl]$^+$.

Structural parameters	[**1**-Cl]$^+$
Ru-Cl (Å)	2.336
$Ru\text{-}P_{(1)}$ (Å)	2.442
$Ru\text{-}P_{(2)}$ (Å)	2.456
$Ru\text{-}C_{(1)}$ (Å)	1.847
$P_{(1)}\text{-}Ru\text{-}P_{(2)}$ (degree)	157.4

Table S4. Structural parameters of first p-complexes of **1a** and **1a**·M^+ with ethene.

Structural parameters	first p-complex of **1a** with ethene	first p-complex of **1a**·Li^+ with ethene	first p-complex of **1a**·K^+ with ethene
$Ru\text{-}Cl_{(1)}$ (Å)	2.475	2.430	2.448
$Ru\text{-}Cl_{(2)}$ (Å)	2.466	2.557	2.518
Ru-P (Å)	2.506	2.485	2.496
$Ru\text{-}C_{(1)}$ (Å)	1.855	1.840	1.844

Ru-$C_{(2)}$ (Å)	2.235	2.261	2.243
Ru-$C_{(3)}$ (Å)	2.253	2.266	2.255
$C_{(2)}$-$C_{(3)}$ (Å)	1.397	1.394	1.397
$C_{(2)}$-Ru-$C_{(3)}$ (degree)	36.3	35.9	36.2
$Cl_{(1)}$-Ru-$Cl_{(2)}$ (degree)	164.3	171.2	170.5
M^+-$Cl_{(2)}$ (Å)	--	2.234	2.967
Ru-$Cl_{(2)}$-M^+ (degree)	--	105.2	108.9
$P_{(1)}$-Ru-$Cl_{(2)}$-M^+ (degree)	--	-103.7	-147.7

Table S5. Structural parameters of Ru-cyclobutane intermediates, the Li^+ and K^+ adduct ions.

Structural parameters	Ru-cyclobutane intermediate	Li^+ adduct ion of Ru-cyclobutane intermediate	K^+ adduct ion of Ru-cyclobutane intermediate
Ru-$Cl_{(1)}$ (Å)	2.460	2.377	2.399
Ru-$Cl_{(2)}$ (Å)	2.426	2.524	2.484
Ru-P (Å)	2.397	2.412	2.405
Ru-$C_{(1)}$ (Å)	2.014	2.024	2.026
Ru-$C_{(3)}$ (Å)	1.980	1.977	1.972
$C_{(1)}$-$C_{(2)}$ (Å)	1.595	1.569	1.575
$C_{(2)}$-$C_{(3)}$ (Å)	1.577	1.593	1.589
$C_{(1)}$-$C_{(2)}$-$C_{(3)}$ (degree)	117.2	117.1	118.0
$C_{(1)}$-Ru-$C_{(3)}$ (degree)	85.4	84.8	85.4
$Cl_{(1)}$-Ru-$Cl_{(2)}$	171.0	174.6	85.4

(degree)			
M^+-$Cl_{(2)}$ (Å)	--	2.219	2.960
Ru-$Cl_{(2)}$-M^+ (degree)	--	100.0	108.7
$P_{(1)}$-Ru-$Cl_{(2)}$-M^+ (degree)	--	-106.0	-92.3

Table S6. Structural parameters of second p-complexes of **4a** and **4a**·M^+ with styrene.

Structural parameters	Second p-complexes of **1a** with styrene	Second p-complexes of **4a**·Li^+ with styrene	Second p-complexes of **4a**·K^+ with styrene
Ru-$Cl_{(1)}$ (Å)	2.473	2.424	2.423
Ru-$Cl_{(2)}$ (Å)	2.455	2.518	2.533
Ru-P (Å)	2.487	2.525	2.486
Ru-$C_{(1)}$ (Å)	2.255	2.317	2.297
Ru-$C_{(2)}$ (Å)	2.295	2.325	2.323
Ru-$C_{(3)}$ (Å)	1.821	1.833	1.823
$C_{(1)}$-$C_{(2)}$ (Å)	1.400	1.407	1.395
$C_{(1)}$-Ru-$C_{(2)}$ (degree)	35.8	35.3	35.2
$Cl_{(1)}$-Ru-$Cl_{(2)}$ (degree)	171.3	171.6	172.8
M^+-$Cl_{(2)}$ (Å)	--	2.173	2.861
Ru-$Cl_{(2)}$-M^+ (degree)	--	70.9	177.4
$P_{(1)}$-Ru-$Cl_{(2)}$-M^+ (degree)	--	144.7	-135.4

Table S7. Structural parameters of **4a** and **4a**·M^+.

Structural parameters	**4a**	**4a**·Li^+	**4a**·K^+
Ru-$Cl_{(1)}$ (Å)	2.350	2.306	2.318
Ru-$Cl_{(2)}$ (Å)	2.344	2.462	2.415
Ru-P (Å)	2.256	2.290	2.280
Ru-$C_{(1)}$ (Å)	1.815	1.812	1.812
$Cl_{(1)}$-Ru-$Cl_{(2)}$ (degree)	144.1	147.5	144.6
M^+-$Cl_{(2)}$ (Å)	--	2.195	2.948
Ru-$Cl_{(2)}$-M^+ (degree)	--	109.1	113.7
$P_{(1)}$-Ru-$Cl_{(2)}$-M^+ (degree)	--	162.0	157.8